

IMT School for Advanced Studies, Lucca

Lucca, Italy

Critical Phenomena in Multilayer Networks

PhD Program in Computer Science and Systems
Engineering

XXXI Cycle

By

Giacomo Rapisardi

2018

Contents

Abstract	5
1 Introduction	1
1.1 Diffusion in complex networks	4
1.2 Phase Transitions in complex networks	7
1.2.1 The Ising model	7
1.2.2 The SIR Model	10
1.2.3 Percolation and network resilience	13
1.3 Single layer vs Multilayer	17
2 Multiple structural transitions in interacting networks	20
2.1 Interconnected networks	20
2.2 Perturbative approach for the spectrum of the graph Laplacian	23
2.2.1 Diagonal interactions (Multiplex)	26
2.2.2 Random interactions	27
2.3 Perturbative approach for the spectrum of the adjacency matrix	32
2.3.1 Random regular and Erdős-Rényi network layers	35
3 Fragility and anomalous susceptibility of weakly interacting networks	38
3.1 Percolation in multilayer networks	38
3.2 The intrinsic powder keg of weakly interacting networks	40

3.3	Model for the anomalous susceptibility and percolation threshold	43
3.4	Real and artificial networks	44
3.5	Finite size scaling	48
3.6	Strongly Interacting Networks	50
4	Numerical Assessment of the percolation threshold using complement networks	54
4.1	Numerical methods and preliminary results	55
4.2	Introduction of the complement graph and further results	57
5	Conclusions	62
A	Perturbation Theory	65
A.1	Nondegenerate Case	65
A.2	Degenerate Case	67
B	Definition and main properties of the complement network	69
	References	71

Abstract

Network science has provided a set of powerful theoretical results for the description of critical phenomena in complex systems. These represent fundamental tools for the design and control of real networked systems with concrete and practical applications. Many of these results have been, however, formulated in the framework of independent networks, *i.e.*, closed systems that do not interact with nor depend on other networks. This is a weak hypothesis because in the real-world networks cannot be considered as independent entities. For instance, critical infrastructure are very often and intentionally coupled together: the functioning of the networks of water and food supply, communications, fuel, financial transactions and power generation and transmission depend one on the other. For this reason, many of the classical results of network science have been questioned, and recent research has provided evidence that many of the results valid for isolated networks are indeed not verified for interacting (or so called *multilayer*) networked systems. With this thesis we present new results in the field of both linear and non-linear dynamical processes in the context of multilayer networks, namely diffusion and percolation. While diffusion is naturally related to the concept of walks and navigability of a network, percolation addresses the concept of stability and resilience of a network under random and targeted attacks.

Chapter 1

Introduction

Complex systems have been one of the main research topic in modern science for the last decades. As a matter of fact most of real-world systems involve large amounts of agents interacting by means of both random and non-random patterns. In several cases these non-trivial interaction structures are able to produce a macroscopic collective behaviour which can hardly be forecast from local microscopic observations: this is indeed one of the fundamental features of a *complex system*. The whole spectrum of properties defining a complex system is in general very broad, and has naturally found uncountable applications in a remarkable variety of more specific disciplines, ranging from physics and economics to biology and sociology. This multidisciplinary aspect, together with the development of modern technologies, led to a growing interest towards complexity science. Indeed the study of complex systems often requires advanced methods in order to both store and manipulate massive amounts of data gathered from real-world systems. These techniques take part in defining the fields of *Big Data* and *Data Science*, thanks to which we now are able to statistically infer relations and dependencies in extrimely large datasets with low information density. However, even tough measuring correlations between observed quantities is crucial and indispensable, mathamatical models are needed in order to have a full understanding of complex systems. One of the most important frame-

works thanks to which we are able to construct such models is given by *Network Theory*.

Loosely speaking a network is a collection of *nodes* (or *vertices*) connected by *links* (or *edges*). In its simplest instance a network is *undirected* and *unweighted*, meaning that links either exist or not exist and do not have a direction. To give a simple example, this picture can be adopted if we want to represent friendships, or generic symmetric relationships among a given number of people. On the other hand many systems require edges to be *weighted*, meaning that every link is associated to a *real* number rather than a *binary* one. Building on the previous example we could define the weight of a relationship to be a function of interaction rates, therefore an edge connecting two close friends would weight more than one connecting two people that barely know each other. We can then further postulate that there are some "famous" people, which are known by the majority of the community, but on the other hand they do not know/interact with each one. This additional information would characterize each link with a specific direction in order to distinguish, in social-networks parlance, "*followers*" from "*following*".

It is therefore understood that networks first of all provide us an incredibly powerful tool in order to visualize the underlying structures of complex systems, but of course this is not the whole story. As a matter of fact each network also defines a particular *topological* space on which complex dynamical processes take place. Our common sense relies on the usual *continuous* 3-dimensional space: every-day physics happens in an environment where, having fixed a reference frame, positions can uniquely be specified by the use of three real numbers named *coordinates*. Since "our" space (even if limited) is continuous, uncountably many positions can be represented, implying that for any two points A and B there exists an infinite amount of ways to connect them. In the case of networks the rules are significantly different: first the space is not continuous, meaning that "points" (nodes) constitute a *countable* set, hence a coordinate system is not required and nodes are instead labeled by an integer i . Moreover the links connecting the nodes form a countable set as well, which implies that the total number of possible paths con-

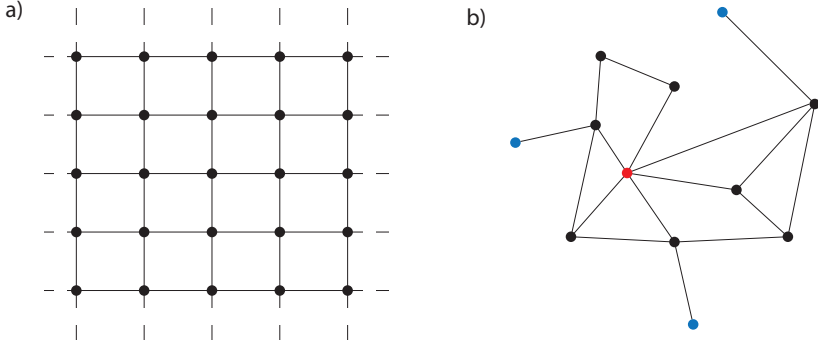


Figure 1: Difference between a generic network (right panel) and a square lattice (left panel). While in the square lattice all nodes have the same degree in the more general case of fig. b) the degree varies from node to node. Here the red node is the *hub*, i.e. the node with the highest degree, while the blue nodes are the *leaves*.

necting A and B is again countable. A simple example of a space with such rules is the square lattice (see fig. 1a), which is a common way to discretize continuous 2-dimensional space. A $N \times N$ square lattice is made of N^2 nodes and, neglecting boundary terms, approximately $2N^2$ edges. Furthermore each node has approximately four neighbors, meaning that starting from point A only four nodes can be reached in one step. In the more general case of a network (fig. 1b) the number of neighbors, which is defined as *degree*, is not the same for every node i : a node with a high degree is called *hub*, while a node with only one connection is usually called *leaf* (see fig. 1). This fundamental topological feature provides a first insight on how a node can be different or, depending on the specific context, *more important* than other nodes. For instance, a random walker in the network of fig.(1b) will likely visit the hub more often with respect to the other nodes. In general, different topologies will significantly affect in different ways the output of dynamical processes taking place in those particular structures. In what follows we show how the specific processes of *diffusion* and *percolation* are described

in the complex-networks environment, and how their general outcome is affected by different topologies. While diffusion is naturally related to the concept of walks and navigability of a network, percolation is deeply related to *phase transitions* theory, and addresses the concept of stability and resilience of a network under random and targeted attacks.

The discussion here is intentionally very elementary and introductory, starting from classic examples from physics and followed by a generalization to the complex-networks environment.

1.1 Diffusion in complex networks

In physics the heat diffusion equation for the state function $u(x, y, z, t)$ is described by the following parabolic partial differential equation:

$$\frac{\partial u}{\partial t} = \alpha \nabla^2 u, \quad (1.1)$$

where ∇^2 is the *Laplacian* differential operator and α is a positive constant. While in continuous 3-dimensional space the Laplacian is given by the *divergence* of the *gradient* (applied to a scalar field), in one dimension it simply reduces to the usual second derivative. Therefore eq. (1.1) in one dimension reads:

$$\frac{\partial u(x, t)}{\partial t} = \alpha \frac{\partial^2 u(x, t)}{\partial x^2}. \quad (1.2)$$

In order to numerically solve equation (1.2) it is a common practice to perform a *discretization* over both space and time. For our purpose here we consider only the space discretization. The continuous x coordinate is then replaced by the discrete index $i \in \mathbb{Z}$, and every component x_i is equally spaced by a fixed small amount Δx . Then, instead of $u(x, t)$ we consider its discretized version $u_i(t)$. Overall, the second derivative is approximated as follows:

$$\frac{\partial^2 u}{\partial x^2} \Big|_{x_i} \simeq \frac{u_{i-1} - 2u_i + u_{i+1}}{\Delta x^2}. \quad (1.3)$$

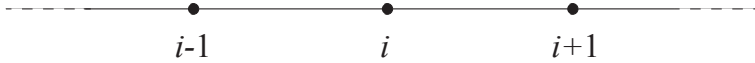


Figure 2: Pictorial representation of the discretized real line.

By using this approximation we can rearrange eq. (1.2) in the following matrix form:

$$\frac{\partial \mathbf{u}(t)}{\partial t} = \alpha' L \mathbf{u}, \quad (1.4)$$

where $\mathbf{u}(t)$ denotes the column vector with components $u_i(t)$, $\alpha' = \alpha/\Delta x^2$ and L is the matrix defined by the following entries:

$$L_{ij} = \begin{cases} -2 & \text{if } i = j \\ 1 & \text{if } j = i + 1 \text{ or } j = i - 1 \\ 0 & \text{otherwise} \end{cases} \quad (1.5)$$

Equation (1.5) defines the Laplacian matrix L . It is immediate to verify that L is symmetrical and has a 0 eigenvalue corresponding to the fixed state $\mathbf{u}_f = (1, 1, 1, \dots)$, which physically speaking corresponds to the state with uniform temperature. Furthermore we can see that L encodes the topology of the discretized real line x (see fig. 2). Indeed we can interpret the discretized real line as a simple network where every node i has two neighbors, namely $i - 1$ and $i + 1$. Hence we can associate each diagonal entry of L to the number of neighbors (or *degree*) of site i and every off-diagonal element of L_{ij} to an edge connecting node i to its following. It is therefore convenient to express L as the difference:

$$L = \mathcal{A} - \mathcal{D}, \quad (1.6)$$

where \mathcal{A} is the *adjacency* matrix

$$\mathcal{A}_{ij} = \begin{cases} 1 & \text{if } i \text{ is connected to } j \\ 0 & \text{otherwise} \end{cases} \quad (1.7)$$

and \mathcal{D} is the diagonal matrix of degrees.

Even though this representation might seem too elaborated for simple heat diffusion in one dimension, it is very important to point out that it can be applied to any kind of topological structure. The adjacency matrix \mathcal{A} defined in eq. (1.7) is a $N \times N$ (with N the number of nodes) binary symmetric matrix which uniquely represents every undirected unweighted graph. To be more general, any real-valued non-symmetric matrix is the representation of certain a directed weighted graph. The association between graphs and adjacency matrices is therefore a one-to-one relationship. Besides that, the diagonal degree matrix \mathcal{D} can be easily derived from \mathcal{A} :

$$\mathcal{D} = \text{Diag}(\mathcal{A}\mathbf{u}_f), \quad (1.8)$$

where \mathbf{u}_f is again the constant 1 column vector defined above.

Having defined the matrices \mathcal{A} and \mathcal{D} we can extend the simple heat-diffusion problem to *any* network. It is customary in the literature to define the Laplacian matrix as

$$\mathcal{L} = \mathcal{D} - \mathcal{A}, \quad (1.9)$$

hence the heat equation takes the form:

$$\frac{\partial \mathbf{x}}{\partial t} = -\alpha \mathcal{L} \mathbf{x}, \quad (1.10)$$

where \mathbf{x} here is the nodes vector.

Thanks to the definition (1.9) the Laplacian matrix \mathcal{L} is, for an undirected unweighted graph, a symmetric semi-positive definite matrix. This implies that all the eigenvalues λ_i are positive real numbers and the evolution of any state $\phi = \sum_i c_i \mathbf{v}_i$, where \mathbf{v}_i are the unit-norm eigenvectors, is governed by:

$$c_i(t) = c_i(0)e^{-\lambda_i t} = c_i(0)e^{t/\tau_i}, \quad (1.11)$$

where the $c_i(0)$ are determined by initial conditions and $\tau_i = \lambda_i^{-1} \forall i$. From eq. (1.11) we clearly see that any given initial state ϕ approach exponentially to the equilibrium state corresponding to the 0 eigenmode. As mentioned above the 0 eigenmode is trivial and is always the same

regardless of the network topology. On the other hand the strictly positive part of the laplacian spectrum determines the speed of convergence towards the equilibrium and depends strongly on the topological features of the network. In particular it is natural to define the *relaxation time* of a network as the largest τ_i , which corresponds to the “slowest” eigenmode. The relaxation time then corresponds to the *second smallest* eigenvalue of the laplacian matrix, which is often denoted as λ_2 . This particular eigenvalue is also known *algebraic connectivity* or *Fiedler value* and its corresponding eigenvector is known as *Fiedler Vector*. The specific value of λ_2 depends on the topology of the network: first $\lambda_2 = 0$ if and only if the network is disconnected, and is upper bounded by the *connectivity* κ (JVM08), that is the minimum number of nodes or edges to be removed in order to disconnect a given graph. Further analytical expressions for the algebraic connectivity can be derived in the case of very specific structures, for instance $\lambda_2 = N$ for a N -nodes complete graph or $\lambda_2 = 2(1 - \cos(\pi/N))$ for a cycle graph with the same number of nodes (NdA07).

In general the algebraic connectivity constitutes a topological quantity of fundamental relevance whose properties have been exploited in many applied research fields ranging from network navigability to synchronization (NAC14; ADGK⁺08) (see Chapter 2 for further details).

1.2 Phase Transitions in complex networks

1.2.1 The Ising model

Another fundamental topic in modern physics is the one of *phase transitions*. In order to have a quick impression on what a phase transition actually is, we start by considering the main steps required to understand the *Ising Model*, which is a fundamental mathematical model of ferromagnetism.

In its simplest instance the Ising model consists in a set of discrete variables $s_i = \pm 1$ representing *magnetic dipole moments* or *spins* arranged in an infinite d -dimensional lattice. The *Hamiltonian function* of the system

(which represents the energy of a given spin configuration) reads:

$$H = -J \sum_{\langle i,j \rangle} s_i s_j - h \sum_i s_i, \quad (1.12)$$

where $J > 0$ is given constant related to interaction strenght, h is a external constant magnetic field and $\sum_{\langle i,j \rangle}$ represents the sum over nearest neighbors.

For our purpose it is sufficient to restrict the problem to the Hamiltonian of one specific spin s_0 :

$$H_{s_0} = -s_0(h + J \sum_i^z s_i), \quad (1.13)$$

where $z = 2d$ here is degree of spin s_0 , *i.e.* the number of nearest neighbors.

Here first we define as *order parameter* the average magnetization $m = \langle s_i \rangle$. The order parameter distinguishes between two possible phases of the system:

- A *nonmagnetic* (disordered) phase where on average each spins variable can assume the value 1 or -1 with same probability, hence $m = 0$.
- An *magnetic* (ordered) phase where the spin values 1 and -1 do not give zero average, hence $m \neq 0$.

As a second step we adopt the common *mean-field* approximation which consists in substituting each random variable s_i with its expectation value m , therefore neglecting fluctuations. The Hamiltonian H_{s_0} can then be approximated by:

$$H_{s_0}^{MF} = -s_0(h + zJm) = -s_0 h_{eff}, \quad (1.14)$$

where we defined the effective field $h_{eff} = h + zJm$.

The goal is to characterize the behavior of the order parameter m as the external temperature T changes. Although the temperature T is not explicitly present in eqs. (1.12) and (1.13), in *equilibrium* statistical mechanics it is assumed that the system is at thermal equilibrium with the

external environment. This assumption, together with other important postulates (Hua87), allows to define a specific measure associating each possible state/configuration σ of the system to a given, temperature-dependent probability P_σ as follows:

$$P_\sigma = \frac{e^{-\frac{H(\sigma)}{k_B T}}}{Z}, \quad (1.15)$$

where k_B is the Boltzmann constant and the normalization term $Z = \sum_{\{\sigma\}} \exp\left[-\frac{H(\sigma)}{k_B T}\right]$ defines the *Canonical partition function*.

In our case the Hamiltonian of eq. (1.13) depends only on the two possible values of the variable s_0 , therefore it is straightforward to compute:

$$\langle s_0 \rangle = \sum_{s_0=\pm 1} s_0 P(s_0) = \tanh\left(\frac{h_{eff}}{k_B T}\right). \quad (1.16)$$

Applying again the mean field argument, hence assuming $\langle s_0 \rangle = m$, finally yields the self-consistent equation:

$$m = \tanh\left(\frac{h + zJm}{k_B T}\right). \quad (1.17)$$

Although equation (1.17) cannot be solved analytically, very important features can be deduced as temperature T decreases, even in the simple case $h = 0$ – hence with no external magnetic field. As we can see from figure (3) there is a particular threshold T_c above which only the solution $m = 0$ exists, while when $T < T_c$ two additional symmetric solutions appear. The critical temperature T_c can be easily obtained by computing the first derivative with respect to m of eq. (1.17) evaluated at $m = 0$, which gives:

$$T_c = \frac{zJ}{k_B} \Rightarrow \beta_c = \frac{1}{zJ}, \quad (1.18)$$

where we adopted the common convention $\beta = [k_B T]^{-1}$.

T_c (or β_c) therefore identifies a critical value that marks a clear boundary between the ordered phase and the disordered one. At this critical point the order parameter is *continuous* but it shows a singularity in its first derivative: for this reason the above described transition is classified as

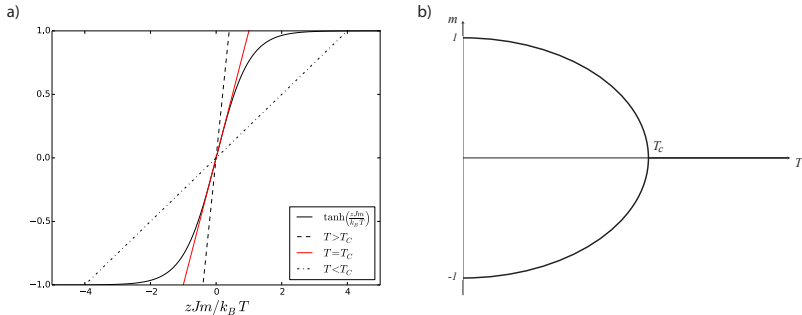


Figure 3: Graphical solution of eq. (1.17) (left panel). As $T < T_c$ two non-trivial solutions appears, giving rise to a second-order phase transition. The whole phase diagram for the two solutions is pictorially represented on the right panel.

a *continuous* or *second-order*¹ phase transition; on the other hand when the order parameter is discontinuous at the critical point the transtion is classified as *first-order* or *discontinuous*.

1.2.2 The SIR Model

Even though the mathematics shown here might seem specific for this very special case, the essential key concepts presented above also apply in other radically different contexts. Indeed, using the same heuristic we could think of representing the spreading of a disease inside a population by replacing lattice sites with individuals and spin variables with health status variables. Then, while in statistical physics time evo-

¹The “*second-order*” expression comes from the original Ehrenfest classification based on the discontinuity of the n -th derivative of the thermodynamic free energy F . In the case of the Ising model the susceptibility $\chi = \frac{\partial^2 F}{\partial h^2}$ diverges at the critical point, while the magnetization $m = \frac{\partial F}{\partial h}$ does not, therefore it is a second-order phase transition according to this definition. In the modern interpretation of critical phenomena, second-order phase transitions are explained in term of *spontaneous symmetry breaking*: for instance in the case of the Ising model this reduces to the fact that for $T < T_c$ the original \mathbb{Z}_2 symmetry for the spin variables is broken, which means $m = \langle s_i \rangle$ assumes a non-zero value.

lution is driven by entropy maximization, in epidemiology there exist several models defining the evolution of the system, but nevertheless very strong analogies appear. Among these models one of the most popular is the *SIR* model, where each individual can be either in state *S* (susceptible), or in state *I* (infected) or in state *R* (removed). For the sake of simplicity let us consider again the mean-field case for the moment, hence every random pair of individuals can interact. Then the susceptibles are infected at a constant rate β , while the infected recovers at a constant rate μ and the recovered cannot be infected anymore. Given $s(t)$, $i(t)$ and $r(t)$ the fraction of susceptible/infected/recovered individuals at time t (hence $s(t) + i(t) + r(t) = 1 \forall t$), we have the nonlinear dynamical system:

$$\frac{di}{dt} = \beta is - \mu i = \mu i \left(\frac{\beta}{\mu} s - 1 \right) \quad (1.19)$$

$$\frac{ds}{dt} = -\beta is \quad (1.20)$$

$$\frac{dr}{dt} = \mu i. \quad (1.21)$$

First we note that from eq. (1.20), for any given initial condition $s(0)$ the function $s(t)$ decreases over time. This implies from eq. (1.19) that if $\frac{\beta}{\mu} s(0) > 1$ there will be an epidemic outbreak while on the contrary there will not. In any case, at the end of the outbreak all the infected individuals will recover, therefore we have the asymptotic condition $i(\infty) = 0$, which implies $r(\infty) + s(\infty) = 1$. We are then interested in finding the asymptotic value $r(\infty)$ in order to characterize the damage of the outbreak. This value can be worked out dividing eq. (1.20) by eq. (1.21), which allows to immediately integrate s as a function of r :

$$s(t) = s(0) \exp \left[-\frac{\beta}{\mu} r(t) \right], \quad (1.22)$$

where for sake of simplicity we reasonably assumed $r(0) = 0$.

By using the above mentioned asymptotic relation we readily get the transcendental equation:

$$r(\infty) = 1 - s(0) \exp [-R_0 r(\infty)], \quad (1.23)$$

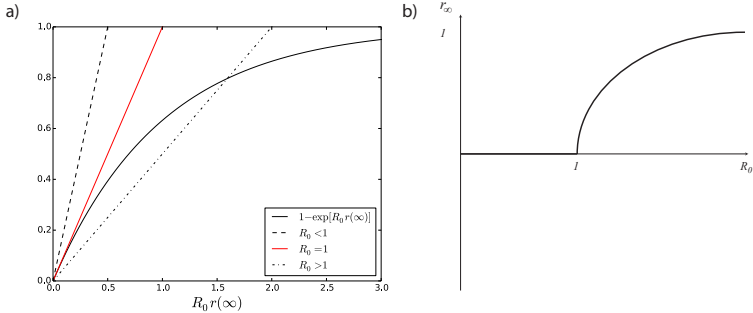


Figure 4: Graphical solution of eq. (1.23) (left panel). $R_0 = 1$ marks a second-order phase transition analogous to the one of figure (3). The phase diagram is pictorially represented on the right panel.

where we defined the *basic reproduction number* $R_0 = \beta/\mu$. Equation (1.23) naturally reminds of the transcendental equation (1.17), especially in the case where $s(0) \simeq 1$. As a matter of fact even if $s(0)$ is very close to 1, if R_0 is larger than 1 there will be an epidemic outbreak, and the particular value $R_0 = 1$ marks a continuous phase transition for the order parameter $r(\infty)$ (see figure 4).

Equations (1.19)(1.20)(1.21) can be straightforwardly generalized to the context of *homogeneous* networks, where each node interacts on average with $\langle k \rangle$ other nodes, where $\langle k \rangle$ is the average degree of the network. The result here is the same of the mean field case, though having redefined $R_0 = \langle k \rangle \beta/\mu$.

A more realistic model is given by the *heterogeneous* (or *degree-based*) mean-field theory (PSCMV14; GDM03). In this context the variables s , i and r are replaced by s_k , i_k and r_k (with $s_k + i_k + r_k = 1$), that are the ratios of susceptible/infected/removed individuals with degree k . The time evolution for this model can be written as (GDM03):

$$\frac{dr_k}{dt} = i_k \quad (1.24)$$

$$\frac{di_k}{dt} = -i_k + \beta k [1 - i_k] \sum_{k'} \frac{k' - 1}{k'} P(k'|k) i_{k'}, \quad (1.25)$$

where without loss of generality we set $\mu = 1$, and $P(k'|k)$ is the probability that a node of degree k has a neighbor of degree k' . Moreover, the factor $(k' - 1)/k'$ in eq. (1.25) takes account of the fact that in the *SIR* model an infected node cannot back-propagate the disease to the neighbor that originally infected it.

For the heterogeneous mean-field *SIR* model, the order parameter is defined as $r_\infty = \sum_k P(k)r_k(\infty)$. In the hypothesis of uncorrelated networks, hence with $P(k'|k) = k'P(k')/k$, by linearization of eqs. (1.25)(1.24) we readily get (PSCMV14; GDM03):

$$\beta_c = \frac{\langle k \rangle}{\langle k^2 \rangle - \langle k \rangle}, \quad (1.26)$$

where all the averages are performed with respect to the measure induced by the degree distribution $P(k)$ – hence $\langle k^2 \rangle = \sum k^2 P(k)$.

From eq. (1.26) we can see how the topology of the network affect the epidemic threshold: in particular if $P(k)$ is Poisson distributed (which the case of classical Erdős-Rényi random graph) we have $R_0 = 1/\langle K \rangle$, while if $P(k) = \delta_{kz}$ (case of regular random graph) we have $R_0 = 1/(z - 1)$. Again these relations remind of eq. (1.18) where the critical value β_c is given by the inverse of the local interaction strength. More interesting is the case of $P(k) = k^{-\gamma}$, hence when the degree distribution is a power-law, which is the topology that characterizes the so-called *scale-free* networks. In particular if we have $\gamma \leq 3$ the second moment of the degree distribution $\langle k^2 \rangle$ diverges, which gives the critical relation $R_0 = 0$. Hence for this particular class of networks even an extremely small value of the infectivity β is sufficient to generate an epidemic outbreak. This last fact is extremely important in order to model epidemics and opinion dynamics among real-world networks. As a matter of fact most of every-day life networks from social networks to the internet itself often show scale-free behavior (CSN09).

1.2.3 Percolation and network resilience

The *SIR* model has been recognized to be equivalent to the process of *bond percolation* (Gra83; New02), that is perhaps one of the simplest math-

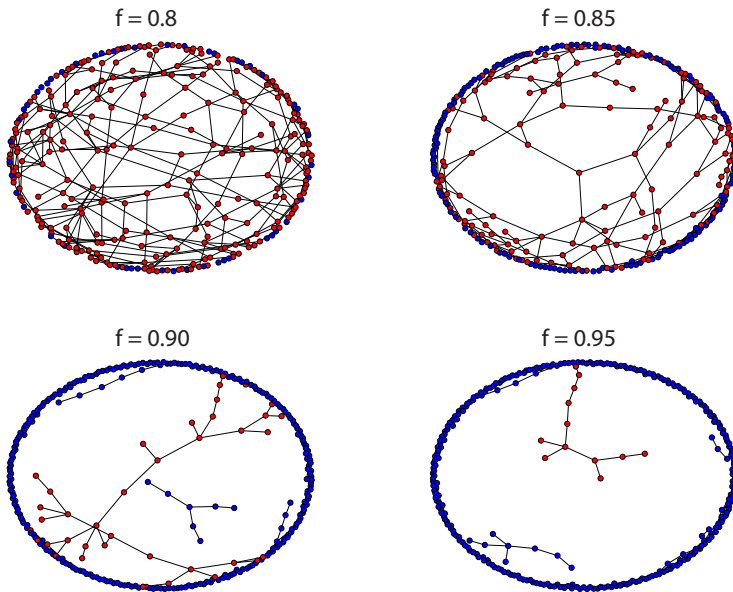


Figure 5: Bond percolation process on an random Erdős-Rényi network of $N = 300$ nodes and average degree $\langle k \rangle = 10$. For each panel the red nodes represent the LCC and f denotes the removed fraction of links.

ematical processes showing a genuine second-order phase transition. In this framework, given a network G , we consider each link to be retained with probability p and removed with probability $f = 1 - p$. On the other hand, the same process applied to nodes rather than links defines *site percolation*. In both cases the goal is to keep track of the relative size S of the graph's Largest Connected Component (LCC) as p varies (see figure 13): the largest the values of S is, the more the network keeps being overall connected. Percolation processes therefore play a fundamental role in describing the *resilience* of a network under random attacks or random failures. Even though the general problem is fairly hard to solve, analytical solutions can be provided in the case of both uncorrelated and loop-free networks using the formalism of generating functions (Wil06).

Let us define as u the probability that a randomly chosen edge e does not belong to the LCC: this happens when either e has been removed (with probability $1 - p$) or when e has not been removed and it is connected to a node which does not belong to the LCC via its adjacent links (e excluded). Therefore the following self-consistent equation can be defined (Wil06; GDM03):

$$u = 1 - p + pg_1(u) \quad \text{with} \quad g_1(u) = \sum_k \frac{(k+1)P(k+1)}{\langle k \rangle} u^k. \quad (1.27)$$

Having solved eq. (1.27), the relative size S of the LCC is then given by:

$$S = p(1 - g_0(u)) \quad \text{with} \quad g_0(u) = \sum_k P(k)u^k. \quad (1.28)$$

Even though (1.27) has to be solved numerically for every considered network, it is possible to derive an analytical threshold for the existence of non trivial solutions. As a matter of fact, while $u = 1$ is always a trivial solution of eq. (1.27), an additional non-trivial solution to the equation may exists since both its left-hand and the right-hand side are defined by two increasing monotone functions and the slope of the right-hand side depends on the external parameter p . Again, this is exactly the same picture of both eq. (1.23) and eq. (1.17). The critical threshold p_c for the existence of a non-trivial solution of eq. (1.27) is found again by computing the derivative with respect to u of both sides evaluated in $u = 1$, which yields:

$$p_c = \frac{1}{g_1'(1)} = \frac{\langle k \rangle}{\langle k^2 \rangle - \langle k \rangle}. \quad (1.29)$$

While $u = 1$ corresponds to $S = 0$ (from eq. (1.28)), for $p > p_c$ we have that S assumes increasing positive values as p gets closer to 1, and the resulting phase diagram is again of the same kind of fig.(4b). Moreover we can clearly see that the critical relations (1.29) and (1.26) are identical. Overall, the set of removed nodes by an *SIR* epidemic outbreak originated from a single node *is equivalent* to the cluster of the bond percolation problem to which the initial node belongs, with $p = 1 - e^{-R_0}$. Given this last fact we know that *bond percolation* and *SIR* epidemic are essen-

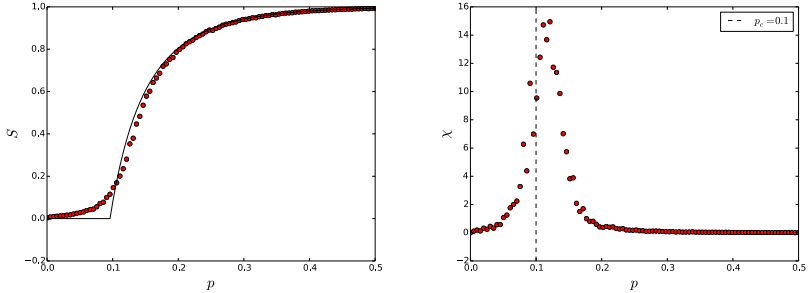


Figure 6: Bond percolation process on an Erdős-Rényi random network with $N = 300$ nodes and average degree $\langle k \rangle = 10$. For each fixed value of the removal probability $1 - p$, the resulting output for S and χ were averaged over 100 realizations of the same process. On the left panel red dots denote the obtained numerical value for S , while the continuous black line represents the numerical solution of eq. (1.28). On the right panel red dots are associated to the numerical output for the susceptibility χ , while the vertical dashed line represents the pseudo-critical threshold of eq. (1.29), which in the case of Erdős-Rényi networks reduces to $p_c = 1/\langle k \rangle = 0.1$.

tially two equivalent problems, both characterized by network’s topology. For instance, as we have seen above, a scale-free network with exponent $\gamma \leq 3$ spreads diseases very easily: on the other hand this feature corresponds to an extreme resilience under random attacks, *i.e.* all links need to be removed in order to dismantle the network completely.

Introduction to finite sizes effects

In all the examples we have seen so far a continuous phase transition is defined by a discontinuity of the order parameter in its first derivative. However the discontinuous behavior of the order parameter holds only in the *thermodynamic* limit, hence when the number of nodes $N \rightarrow \infty$. Discontinuities are in general *smoothed* by finite-size effects (see figure 6a). In the context of locally tree-like networks (hence for networks with a decreasing loop density as N increases), eq. (1.29) rather defines a *pseudo-critical* threshold $p_c(N)$ which approaches the *real* percolation

threshold only in the thermodynamic limit. In order to have the best numerical estimate of the percolation threshold it is customary to compute the numerical *susceptibility* χ , which can be defined as:

$$\chi = \frac{\text{Var}(S)}{\langle S \rangle}, \quad (1.30)$$

where here the average is defined on the set of random realizations of the percolation process at fixed removal probability $1 - p$. While in the thermodynamic limit the susceptibility χ diverges as $p \rightarrow p_c$, at all finite sizes χ does not diverge around the critical point, but it rather reaches a maximum χ_{max} . Therefore χ_{max} is a common way to give a best numerical estimate of the percolation transition at finite sizes (see figure 6b).

In general on a finite network of size N , the order parameter scales according in the following way (RC15a):

$$B = N^{-\frac{\beta}{\nu}} F(|p - p_c| N^{\frac{1}{\nu}}), \quad (1.31)$$

where $\beta, \nu > 0$ are two positive constants named *critical exponents* and F is a scaling function. Moreover for the pseudo-critical threshold $p_c(N)$ we have the following power law decay towards the real threshold p_c (RC15a):

$$p_c(N) - p_c \propto N^{\frac{1}{\nu}}. \quad (1.32)$$

Overall, at $p = p_c(N)$ we have $S \sim N^{\beta/\nu}$ and $\chi_{max} \sim N^{1-\beta/\nu}$. The particular values for the critical exponents depend on the network topology and identify the so-called *universality classes*, which describe in a universal manner the critical percolation properties of different kind of networks (see (DGM08) for further details).

1.3 Single layer vs Multilayer

In the previous sections we have stressed several times how the output of a dynamical process is affected by the topology of the network in which takes place, however we mainly focused on the effect of the degree distribution $P(k)$ and its first moments, such as the average degree $\langle k \rangle$. For

instance, eq. (1.29) holds under the locally-tree like ansatz, hence when any loop-effect is avoided. Indeed, the effect of higher-order topological properties such as the *clustering coefficient* (which is related to the density of closed triangles in the graph) is still an argument of debate, especially in the field of percolation (SBn06; RC16a). Nevertheless lower-order properties are able to satisfactorily cover a large number of cases, except when we deal with *multi-layer* networks. In fact multilayer networks are characterized by a given number of networks (called *layers*) and an interconnection structure between the layers. In many real-life systems it is often needed to differentiate between the type of interconnections: for insistance, two friends might follow each other in Twitter while they might not in Instagram, or cities that might be connected or not when different airlines companies are considered. These cases present more information to be encoded in our mathematical formalism: indeed, the adjacency matrix is often substituted by higher dimensional objects such *adjancency tensors* (DDSRC⁺13; DDGPA16) or *supra-adjacency* matrices (see next chapter). Multilayer networks have been deeply investigated in recent years, showing critical properties not accessible to single layer structures, such as structural transition as well as multiple, discontinuous and hybrid phase transition.

A more detailed treatment of multilayer networks will be given in the next chapters. In particular, Chapter (2) reports our recent work on multiple structural transitions in interacting networks (RACC18b). In this work, thanks to the use of first order perturbation theory, we generalize previous results reporting a single structural transition in the algebraic connectivity to the more general result of z multiple structural transition, where z is the number of network layers.

Chapter (3) reports our latest contribution in the field of percolation in multilayer networks (RACC18a). In particular we deal with the specific case of weakly-incterconnected networks, showing an anomalous behavior of the observed susceptibility caused by random abrupt jumps in the order parameter. Moreover, a finite-size scaling analysis in the abrupt region supports the hypothesis of a genuine first-order phase transition.

Finally in Chapter (4) we present a recent in-depth study on bond percolation which aims to exploit the information provided by the *complement* of a given graph in order to numerically construct better estimates for the bond percolation threshold. The method presented may be applied to both single and multilayer networks (RGG19).

We conclude with a discussion on the importance of results and future developments in Chapter (5).

Chapter 2

Multiple structural transitions in interacting networks

2.1 Interconnected networks

Interconnected (or interdependent) networks are a natural representation of complex systems composed by several networks interacting with each other (DDSRC⁺¹³; KAB⁺¹⁴; BBC⁺¹⁴; Gar16). It is known that those interactions are able to make such systems significantly different from isolated networks by both a structural and dynamical point of view (Rad14; DDGPA16). As a matter of fact dissimilar behaviours have been reported in navigability (DDSRGA14), communicability (EGGn14), robustness (BPP⁺¹⁰; GBHS11; GGDDG⁺¹⁵), percolation (HKCH11; BD14; HCG⁺¹⁶), epidemics (SMSBn12; DHS12; WX12a; GGA13), and synchronization (HPL⁺⁰⁶; ASEG⁺¹⁴).

Within the field of interconnected networks, the Laplacian matrix constitutes a fundamental mathematical object to which much attention has been devoted recently (RA13; GDGGGn⁺¹³; SRDDK⁺¹³; MHWMD14; SGCM14; DSSVM15; SADS⁺¹⁶; VM16). Given an undirected graph G , the Laplacian matrix \mathcal{L} is defined as $\mathcal{D} - \mathcal{A}$, where \mathcal{A} is the adjacency ma-

trix of G (its generic element $\mathcal{A}_{ij} = 1$ if i and j are connected, and $\mathcal{A}_{ij} = 0$ otherwise) and \mathcal{D} is the diagonal matrix of degrees, which we write as $\mathcal{D} = \text{diag}(\mathcal{A}|1\rangle)$, where $|1\rangle$ denotes the column vector with all entries equal to 1¹. Since the Laplacian matrix can also be written as $\mathcal{L} = \mathcal{M}^T \mathcal{M}$ (where \mathcal{M} is the network incidence matrix²), it trivially follows that \mathcal{L} is positive semidefinite, meaning that all of its eigenvalues are non-negative. Furthermore by construction row/column sums of \mathcal{L} are all zero, in fact $\mathcal{L}|1\rangle = \mathcal{A}|1\rangle - \mathcal{A}|1\rangle = |0\rangle$. The Laplacian matrix therefore always admits $\lambda_1(\mathcal{L}) = 0$ as the smallest eigenvalue, corresponding to the eigenvector $|1\rangle$. The second-smallest eigenvalue of the spectrum, $\lambda_2(\mathcal{L})$, defined as the *algebraic connectivity* of the graph, reflects how much connected the overall graph is (Fie75). Indeed, $\lambda_2(\mathcal{L})$ is different from zero if and only if the graph is connected; otherwise, its degeneracy equals the number of disconnected components of the graph. The value of $\lambda_2(\mathcal{L})$ is determined as:

$$\lambda_2(\mathcal{L}) = \min_{|v\rangle \in \mathcal{V}} \langle v | \mathcal{L} | v \rangle \quad (2.1)$$

where $|v\rangle \in \mathcal{V}$ is such that $\langle v | 1 \rangle = 0$ and $\langle v | v \rangle = 1$, and \mathcal{V} is the set of normalized eigenvectors of \mathcal{L} .

The Laplacian spectrum is typically used in order to characterize both structural properties of the networked system, such as connectivity, diameter and number of spanning trees (Moh91; JVM08), as well as dynamical properties, such as diffusion and synchronization (ADG07; ADGK⁺08; SDM08). Recently, Radicchi and Arenas (RA13) showed that the process of building independent network layers into a multiplex network—which is a peculiar type of multilayer interconnected network in which nodes replicate at each layer—undergoes a structural transition in the algebraic connectivity as interconnections are formed. Specifically, let us define $q \in [0, 1]$ as the interaction strength between two network layers, meaning that we assign the same weight q to every interconnection link. It was shown (RA13) that $\lambda_2(q)$ is an increasing monotonic

¹In this chapter we adopt the bra-ket notation, hence $|v\rangle$ indicates a generic column vector while $\langle v| = |v\rangle^T$ indicates a generic row vector.

²The incidence matrix \mathcal{M} is of size $N \times E$ (with N the number of nodes and E the number of edges) and has entries $\mathcal{M}_{ij} = 1$ if *node* i and *edge* j are incident and 0 otherwise.

function which presents a sharp critical point q_c at which $\partial\lambda_2/\partial q$ is discontinuous. For $q < q_c$ the two networks are structurally distinguishable (and the system behavior is not affected by their detailed topology but depends only on the interconnection structure), whereas, for $q > q_c$ the interconnected network functions as a whole (and topological effects do play a role). Later, Darabi Sahneh *et al.* (DSSVM15) found an exact solution for q_c . Moreover, they observed that the structural transition disappears when one of the network layers has vanishing algebraic connectivity: layers of such interconnected network topologies become indistinguishable, despite very weak coupling between them. Martín-Hernández *et al.* (MHWMD14) further showed that, for a multiplex, there exists a critical number of diagonal interlinks beyond which any further inclusion does not enhance the algebraic connectivity of the system at all, whereas, for a randomly interconnected system, there exists a critical number of random interlinks beyond which algebraic connectivity increments at half of the original rate. Van Mieghem (VM16) further computed the nontrivial eigenmode of the Laplacian for a regular topological structure of interconnections.

In what follows we blend this research line of studying structural transitions in interacting networks. In order to tackle general topologies of both network layers and interconnections we use the approximation given by first order perturbation theory. Perturbation theory has already found several application in network science, for instance to study the Laplacian eigenvalues of scale-free networks (KM07), to analyze spectral properties of networks with community structure (CGO09), to identify important nodes within communities (WDF11), to find the relation between eigenvector and topological perturbations (YWL⁺14), to analyze the localization properties of Laplacian eigenvectors on random networks (HN17) and, in the context of multiplex networks, to unveil the time scales of diffusive processes (GDGGGn⁺13; SRDDK⁺13). The underlying idea of perturbation theory is to treat an operator acting on the system as the sum of an *unperturbed* part, which in our context refers to isolated network layers and for which the exact solution may exist, and a *perturbation*, given by the interconnections between these layers. For a

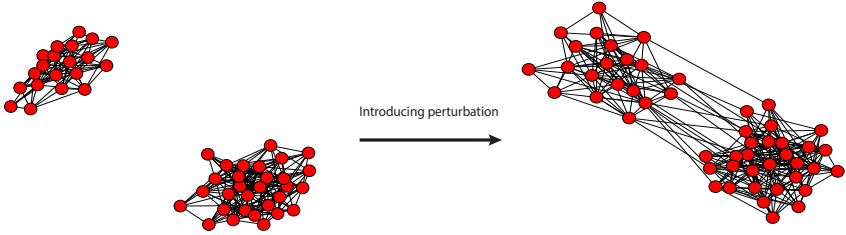


Figure 7: Pictorial representation of the *unperturbed* system (disconnected networks) and the *perturbed* one (interconnected networks).

more detailed treatment of perturbation theory see Appendix A.

Our proposal constitutes a very general framework for the analysis of structural transitions in the most wide scope of interconnected/interdependent multilayer networks. The analytical characterization of such transitions in this approximation regime represents a step forward in the direction of having a closed theory of multilayer networks.

2.2 Perturbative approach for the spectrum of the graph Laplacian

We focus on studying the variation of the Laplacian matrix spectrum when the perturbation is introduced. The perturbation here is naturally identified with the introduction of the interconnection links (see figure 7). We start with the simplest case of two connected, undirected unweighted networks \mathcal{A} and \mathcal{B} , with N and M nodes each, respectively. Interconnections are randomly established between these networks, and are described by a generic $N \times M$ adjacency matrix \mathcal{Q} . The supra-Laplacian of the whole system can be represented with the four-blocks $(N + M) \times (N + M)$ matrix (RA13):

$$\mathcal{L} = \begin{pmatrix} \mathcal{L}_{\mathcal{A}} + \mathcal{K}_{\mathcal{A}} & -\mathcal{Q} \\ -\mathcal{Q}^T & \mathcal{L}_{\mathcal{B}} + \mathcal{K}_{\mathcal{B}} \end{pmatrix}, \quad (2.2)$$

where \mathcal{L}_A and \mathcal{L}_B are the Laplacian matrices of each network, while $\mathcal{K}_A = \text{diag}(Q|1)$ and $\mathcal{K}_B = \text{diag}(Q^T|1)$ are the diagonal matrices of inter-degrees. To apply perturbation theory, we split \mathcal{L} into an unperturbed part \mathcal{L}_0 and a perturbation \mathcal{V} :

$$\mathcal{L} = \mathcal{L}_0 + \mathcal{V} = \begin{pmatrix} \mathcal{L}_A & 0 \\ 0 & \mathcal{L}_B \end{pmatrix} + \begin{pmatrix} \mathcal{K}_A & -Q \\ -Q^T & \mathcal{K}_B \end{pmatrix}. \quad (2.3)$$

We denote, for \mathcal{L}_0 , the unperturbed spectrum of eigenvalues as $E_n^{(0)}$ and its associated orthonormal basis of eigenvectors as $|n^{(0)}\rangle$. Without loss of generality we can write the unperturbed spectrum as:

$$E_n^{(0)} = \{0, 0, \lambda_2(\mathcal{L}_A), \lambda_2(\mathcal{L}_B), \dots\}, \quad (2.4)$$

where $\lambda_2(\mathcal{L}_A)$ and $\lambda_2(\mathcal{L}_B)$ are the algebraic connectivities of layer A and B respectively. Note that in this case we have a 2-fold degeneracy in the 0 eigenvalue, since by definition the unperturbed system consists of two disconnected components. After having introduced the interconnection matrix Q the full spectrum reads:

$$E_n = \{\epsilon_0, \epsilon_1, \lambda_2(\mathcal{L}_A) + \epsilon_2, \lambda_2(\mathcal{L}_B) + \epsilon_3, \dots\}, \quad (2.5)$$

where ϵ_n is the correction to the n -th eigenvalue of the unperturbed spectrum. Perturbation theory then consists in defining for each n the following series:

$$\epsilon_n = \epsilon_n^{(1)} + \epsilon_n^{(2)} + \epsilon_n^{(3)} + \dots, \quad (2.6)$$

where we define $\epsilon_n^{(1)}$ to be the *first order* correction, $\epsilon_n^{(2)}$ the *second order* correction and so on (see Appendix A for further details).

For the non-degenerate part of $E_n^{(0)}$ first-order correction reads:

$$\epsilon_n^{(1)} = \langle n^{(0)} | \mathcal{V} | n^{(0)} \rangle, \quad (2.7)$$

so that the spectrum of \mathcal{L} at first order would be simply given by:

$$E_n^{(1)} = E_n^{(0)} + \langle n^{(0)} | \mathcal{V} | n^{(0)} \rangle. \quad (2.8)$$

However we have to resolve the 2-fold degeneracy in the 0 eigenvalue for \mathcal{L}_0 . In order to do so we can introduce the unperturbed eigenstates:

$$\begin{aligned} |+\rangle^{(0)} &= \frac{1}{\sqrt{N+M}} \begin{pmatrix} |1\rangle \\ |1\rangle \end{pmatrix} \\ |-\rangle^{(0)} &= \frac{1}{\sqrt{N+M}} \begin{pmatrix} \sqrt{\frac{M}{N}} |1\rangle \\ -\sqrt{\frac{N}{M}} |1\rangle \end{pmatrix} \end{aligned}$$

as the orthonormal basis for such a degenerate sub-space (VM16). Since the perturbation \mathcal{V} becomes diagonal when represented in this basis (*i.e.*, $\langle +^{(0)} | \mathcal{V} | -^{(0)} \rangle = \langle -^{(0)} | \mathcal{V} | +^{(0)} \rangle = 0$), we immediately get the eigenvalues corresponding to $|+\rangle^{(0)}$ and $|-\rangle^{(0)}$:

$$\epsilon_0^{(1)} = \langle +^{(0)} | \mathcal{V} | +^{(0)} \rangle = 0, \quad (2.9)$$

$$\epsilon_1^{(1)} = \langle -^{(0)} | \mathcal{V} | -^{(0)} \rangle = \frac{\tau(\mathcal{Q})}{\mu}, \quad (2.10)$$

where $\tau(\mathcal{Q}) = \langle 1 | \mathcal{Q} | 1 \rangle \equiv \sum_{ij} Q_{ij}$ and $\mu = NM/(N+M)$. Note that $\epsilon_1^{(1)}$ depends only on N , M and $\tau(\mathcal{Q})$ (which is just the total number of interconnection links). Remarkably, eq. (2.9) reminds of the classical two-body problem of two masses N and M mutually interacting by means of a coupling force of intensity $\tau(\mathcal{Q})$ (VM16): $\epsilon_0^{(1)}$ gives the acceleration for the center of mass while $\epsilon_1^{(1)}$ is the relative acceleration between the two masses.

We then consider the smallest non-zero eigenvalues of the unperturbed state \mathcal{L}_0 given by the algebraic connectivities of either network \mathcal{A} or \mathcal{B} . Denoting as $|v_{\mathcal{A}}\rangle$ the Fiedler vector of network \mathcal{A} , that is the normalized eigenvector corresponding to $\lambda_2(\mathcal{L}_{\mathcal{A}})$, we pose $|v_{\mathcal{A}}^{(0)}\rangle = \begin{pmatrix} |v_{\mathcal{A}}\rangle \\ |0\rangle \end{pmatrix}$. The first order correction to $\lambda_2(\mathcal{L}_{\mathcal{A}})$ is, according to both eq. (2.7) and the notation adopted in eq. (2.5)

$$\epsilon_2^{(1)} = \langle v_{\mathcal{A}}^{(0)} | \mathcal{V} | v_{\mathcal{A}}^{(0)} \rangle \equiv \langle v_{\mathcal{A}} | \mathcal{K}_{\mathcal{A}} | v_{\mathcal{A}} \rangle. \quad (2.11)$$

Analogously, denoting as $|v_{\mathcal{B}}\rangle$ the Fiedler vector of network \mathcal{B} , and posing $|v_{\mathcal{B}}^{(0)}\rangle = \begin{pmatrix} |0\rangle \\ |v_{\mathcal{B}}\rangle \end{pmatrix}$, we have:

$$\epsilon_3^{(1)} = \langle v_{\mathcal{B}}^{(0)} | \mathcal{V} | v_{\mathcal{B}}^{(0)} \rangle \equiv \langle v_{\mathcal{B}} | \mathcal{K}_{\mathcal{B}} | v_{\mathcal{B}} \rangle. \quad (2.12)$$

Hence, the first order correction to the algebraic connectivity of \mathcal{A} and \mathcal{B} is given only by the degree configuration of the perturbation term projected on the Fiedler vector of $\mathcal{L}_{\mathcal{A}}$ and $\mathcal{L}_{\mathcal{B}}$ respectively, independently on the particular topology of this perturbation term. Thus, both Eqs. (2.11) and (2.12) can be lower and upper bounded by the minimum and maximum interdegree connectivity, whereas $\lambda_2(\mathcal{L}_{\mathcal{A}})$ and $\lambda_2(\mathcal{L}_{\mathcal{B}})$ can be upper bounded by the minimum degrees of layer \mathcal{A} and \mathcal{B} , respectively (JVM08).

Overall, at first order in perturbation theory we have:

$$\lambda_2(\mathcal{L}) = \min \left\{ \frac{\tau(\mathcal{Q})}{\mu}, \lambda_2(\mathcal{L}_{\mathcal{A}}) + \langle v_{\mathcal{A}} | \mathcal{K}_{\mathcal{A}} | v_{\mathcal{A}} \rangle, \lambda_2(\mathcal{L}_{\mathcal{B}}) + \langle v_{\mathcal{B}} | \mathcal{K}_{\mathcal{B}} | v_{\mathcal{B}} \rangle \right\}. \quad (2.13)$$

Since $\epsilon_1^{(1)}$ is the correction to the zero eigenvalue, we have that if $\tau(\mathcal{Q})$ is small enough then $\lambda_2(\mathcal{L}) = \epsilon_1^{(1)}$. In this phase the algebraic connectivity depends only on both the total number of interconnection links and the sizes of the two interacting networks \mathcal{A} and \mathcal{B} , meaning that it is *not affected* by their topology. However, when $\tau(\mathcal{Q})$ grows, the second and third smallest eigenvalues of the interacting network might swap (MHWMD14). This happens when

$$\tau(\mathcal{Q})/\mu = \min \{ \lambda_2(\mathcal{L}_{\mathcal{A}}) + \langle v_{\mathcal{A}} | \mathcal{K}_{\mathcal{A}} | v_{\mathcal{A}} \rangle, \lambda_2(\mathcal{L}_{\mathcal{B}}) + \langle v_{\mathcal{B}} | \mathcal{K}_{\mathcal{B}} | v_{\mathcal{B}} \rangle \}.$$

Note that if one of the networks \mathcal{A} and \mathcal{B} has a vanishing algebraic connectivity, the transition point disappears (VM16). This happens, *e.g.*, for a class of scale-free networks where $\lambda_2(\mathcal{L}_{\mathcal{A}}) \sim (\ln N)^{-2}$ (SDM08). Importantly, an additional swapping may also occur for the algebraic connectivities of the two network layers, *i.e.*, when and if

$$\lambda_2(\mathcal{L}_{\mathcal{A}}) + \langle v_{\mathcal{A}} | \mathcal{K}_{\mathcal{A}} | v_{\mathcal{A}} \rangle = \lambda_2(\mathcal{L}_{\mathcal{B}}) + \langle v_{\mathcal{B}} | \mathcal{K}_{\mathcal{B}} | v_{\mathcal{B}} \rangle.$$

To get a qualitative insight on the system behavior, in the following we consider two particular situations, diagonal and random interactions.

2.2.1 Diagonal interactions (Multiplex)

In a multiplex network, \mathcal{A} and \mathcal{B} have the same number of nodes ($N = M$) and $\mathcal{Q} = q\mathcal{I}$ is proportional to the $N \times N$ identity matrix. While

the minimization problem of eq. (2.1) can be solved exactly in this case (RA13; DSSVM15), using perturbation theory leads to:

$$\lambda_2(\mathcal{L}) = q + \min \{q, \lambda_2(\mathcal{L}_A), \lambda_2(\mathcal{L}_B)\}. \quad (2.14)$$

Since the ordering of $\lambda_2(\mathcal{L}_A)$ and $\lambda_2(\mathcal{L}_B)$ is fixed, there is only one eigenvalue swapping at $q_c \simeq \min \{\lambda_2(\mathcal{L}_A), \lambda_2(\mathcal{L}_B)\}$.

When the two networks \mathcal{A} and \mathcal{B} are identical, then $\lambda_2(\mathcal{L}_A) = \lambda_2(\mathcal{L}_B)$. Resolving this additional degeneracy with eigenvectors $\frac{1}{\sqrt{2}} \begin{pmatrix} |v_A\rangle \\ |v_A\rangle \end{pmatrix}$ and $\frac{1}{\sqrt{2}} \begin{pmatrix} |v_A\rangle \\ -|v_A\rangle \end{pmatrix}$ leads to first order corrections for $\lambda_2(\mathcal{L}_A)$ equal to 0 and $2q$, hence $q_c \simeq \lambda_2(\mathcal{L}_A)/2$ (it is halved with respect to the non-degenerate case) (MHWMD14). Furthermore, note that in this particular case first order approximation is exact, meaning that $\epsilon_n^{(1)} = \epsilon_n \forall n$. As a matter of fact in this case \mathcal{L}_0 commutes with perturbation \mathcal{V} , therefore the same unperturbed set of orthonormal eigenvectors $|n^{(0)}\rangle$ diagonalizes \mathcal{L}_0 and \mathcal{V} simultaneously, implying that the correction given by eq. (2.7) is exactly the difference between the perturbed spectrum E_n and the unperturbed one $E_n^{(0)}$. To prove that $[\mathcal{L}_0, \mathcal{V}] = 0$, since \mathcal{L}_0 and \mathcal{V} are symmetric matrices, it is sufficient to verify that $\mathcal{L}_0\mathcal{V}$ is symmetric³:

$$\mathcal{L}_0\mathcal{V} = \begin{pmatrix} \mathcal{L}_A & 0 \\ 0 & \mathcal{L}_B \end{pmatrix} \begin{pmatrix} q\mathcal{I} & -q\mathcal{I} \\ -q\mathcal{I} & q\mathcal{I} \end{pmatrix} = q \begin{pmatrix} \mathcal{L}_A & \mathcal{L}_A \\ \mathcal{L}_B & \mathcal{L}_B \end{pmatrix},$$

therefore $\mathcal{L}_0\mathcal{V}$ is symmetric only if $\mathcal{L}_A = \mathcal{L}_B$.

2.2.2 Random interactions

A more general situation is described by an $N \times M$ interaction matrix \mathcal{Q} assuming the form of an Erdős-Rényi random graph with connection probability q . This setting resembles that of an individual network with two communities \mathcal{A} and \mathcal{B} which are randomly interconnected (CGO09). In order to proceed, we use a mean field approximation by replacing all matrix elements Q_{ij} with their expectation value q . Again in this regime \mathcal{L}_0 commutes with \mathcal{V} , implying that first-order approximation is exact.

³ Given two symmetric matrices A and B their product AB is symmetric if and only if A commutes with B .

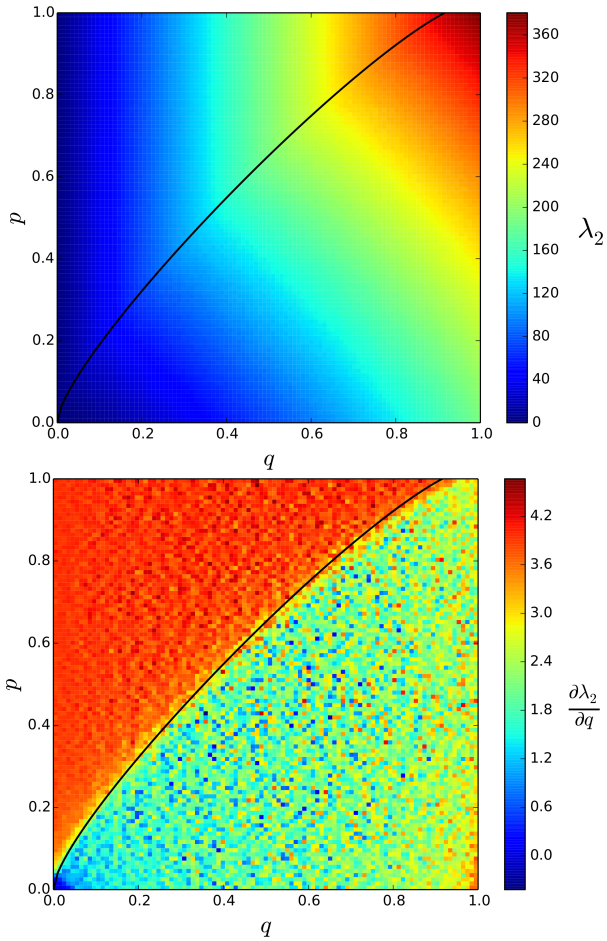


Figure 8: Heat-map of $\lambda_2(\mathcal{L})$ (upper panel) and of $\partial\lambda_2(\mathcal{L})/\partial q$ (lower panel) for two interacting Erdős-Rényi graphs of $N = 200$ nodes each and link probability p . The solid line is the curve described by eq. (2.16).

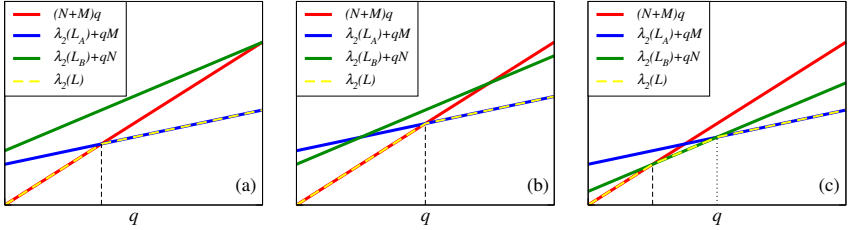


Figure 9: Behavior of $\lambda_2(\mathcal{L})$ given by eq. (2.15) for $M < N$ and: (a) $\lambda_2(\mathcal{L}_A) < \lambda_2(\mathcal{L}_B)$; (b) $\lambda_2(\mathcal{L}_A) > \lambda_2(\mathcal{L}_B)$ and $\lambda_2(\mathcal{L}_A)/N < \lambda_2(\mathcal{L}_B)/M$; (c) $\lambda_2(\mathcal{L}_A) > \lambda_2(\mathcal{L}_B)$ and $\lambda_2(\mathcal{L}_A)/N > \lambda_2(\mathcal{L}_B)/M$. Vertical dashed and dotted lines mark q_c and q'_c , respectively.

Indeed, verifying that $\mathcal{L}_0\mathcal{V}$ is symmetric is again quite straightforward:

$$\begin{aligned} \mathcal{L}_0\mathcal{V} &= \begin{pmatrix} \mathcal{L}_A & 0 \\ 0 & \mathcal{L}_B \end{pmatrix} \begin{pmatrix} Mq\mathcal{I}_N & -q|1_N\rangle\langle 1_M| \\ -q|1_M\rangle\langle 1_N| & Nq\mathcal{I}_M \end{pmatrix} = \\ &= \begin{pmatrix} Mq\mathcal{L}_A & 0 \\ 0 & Nq\mathcal{L}_B \end{pmatrix}, \end{aligned}$$

where $|1_N\rangle$ and $|1_M\rangle$ denote the constant 1 vectors of dimension N and M respectively, and $\mathcal{I}_{N,M}$ is the N or M dimensional identity matrix. Note that in order to get this result we used the general fact that $\mathcal{L}|1\rangle = 0$. Overall, for this particular setting eq. (2.13) becomes:

$$E[\lambda_2(\mathcal{L})] = \min \{(N+M)q, \lambda_2(\mathcal{L}_A) + qM, \lambda_2(\mathcal{L}_B) + qN\}. \quad (2.15)$$

Again in the special case of \mathcal{A} and \mathcal{B} identical (which also implies $N = M$), resolving the degeneracy $\lambda_2(\mathcal{L}_A) = \lambda_2(\mathcal{L}_B)$ with eigenvectors $\frac{1}{\sqrt{2}}\begin{pmatrix} |v_A\rangle \\ |v_A\rangle \end{pmatrix}$ and $\frac{1}{\sqrt{2}}\begin{pmatrix} |v_A\rangle \\ -|v_A\rangle \end{pmatrix}$ leads to first order corrections both equal to Nq , so that also in this case there is only one eigenvalue swapping at $q_c \simeq \lambda_2(\mathcal{L}_A)/N$ (MHWMD14). Under the mean-field approximation, these conclusions hold also if the two networks are identical on expectation. For instance, consider \mathcal{A} and \mathcal{B} to be Erdős-Rényi random graphs with the same number of nodes and connection probability p . In order to have an analytical estimate for the algebraic connectivities we first approximate $\lambda_2(\mathcal{A})$ and $\lambda_2(\mathcal{B})$ with the minimum degree of networks

\mathcal{A} and \mathcal{B} respectively ⁴ (JVM08) and then we use the approximation of the minium degree of an Erdős-Rényi graph which can be deduced from (Bol81). Dropping terms below $O(\sqrt{N \log N})$, we have

$$E[\lambda_2(\mathcal{L}_{\mathcal{A}})] = E[\lambda_2(\mathcal{L}_{\mathcal{B}})] \simeq Np - \sqrt{2p(1-p)N \log N},$$

hence

$$q_c \approx p - \sqrt{2p(1-p)(\log N)/N} \quad (2.16)$$

(see Fig. 8). In the limit $N \rightarrow \infty$, $q_c \rightarrow p$ as $\sqrt{\log N/N}$: the transition at q_c is therefore well defined even in the thermodynamic limit.

To discuss the more general setting of \mathcal{A} and \mathcal{B} having different sizes and topologies, without loss of generality we set $M < N$. Then if $\lambda_2(\mathcal{L}_{\mathcal{A}}) < \lambda_2(\mathcal{L}_{\mathcal{B}})$, eq. (2.15) tells us that the algebraic connectivity of \mathcal{A} grows at a slower rate than that of \mathcal{B} , and they never become equal: only one eigenvalue swapping is possible, occurring again at

$$q_c = \lambda_2(\mathcal{L}_{\mathcal{A}})/N. \quad (2.17)$$

Instead if $\lambda_2(\mathcal{L}_{\mathcal{A}}) > \lambda_2(\mathcal{L}_{\mathcal{B}})$, the first eigenvalue swapping occurs at $q_c = \min \{ \lambda_2(\mathcal{L}_{\mathcal{A}})/N, \lambda_2(\mathcal{L}_{\mathcal{B}})/M \}$. Moreover, also the two algebraic connectivities of \mathcal{A} and \mathcal{B} swap at

$$q'_c = \frac{\lambda_2(\mathcal{L}_{\mathcal{A}}) - \lambda_2(\mathcal{L}_{\mathcal{B}})}{N - M}. \quad (2.18)$$

Such a transition is actually observed for $\lambda_2(\mathcal{L})$ only when $q_c < q'_c$, implying $\lambda_2(\mathcal{L}_{\mathcal{A}})/N > \lambda_2(\mathcal{L}_{\mathcal{B}})/M$ and when $q'_c < 1$, implying $\lambda_2(\mathcal{L}_{\mathcal{A}}) + M < \lambda_2(\mathcal{L}_{\mathcal{B}}) + N$. Figure 9 illustrates the different situations. Note that the second transition happens even for $\lambda_2(\mathcal{L}_{\mathcal{B}}) \rightarrow 0$ (*i.e.*, when \mathcal{B} is a scale-free network): $q_c \rightarrow 0$ but $q'_c \neq 0$, provided $\lambda_2(\mathcal{L}_{\mathcal{A}})$ remains finite yet smaller than $N - M$. The phase diagram of Fig. 10 refers instead to \mathcal{A} and \mathcal{B} being Erdős-Rényi random graphs with connection probabilities p_A and p_B respectively. In the thermodynamic limit and for $r = M/N < 1$ finite, for $p_A < p_B$ one transitions is observed at $q_c \simeq p_A$, whereas, for $p_A > p_B$

⁴In general $\lambda_2 \leq \kappa < k_{min}$, where κ is the graph connectivity and k_{min} is the minimum degree (JVM08).

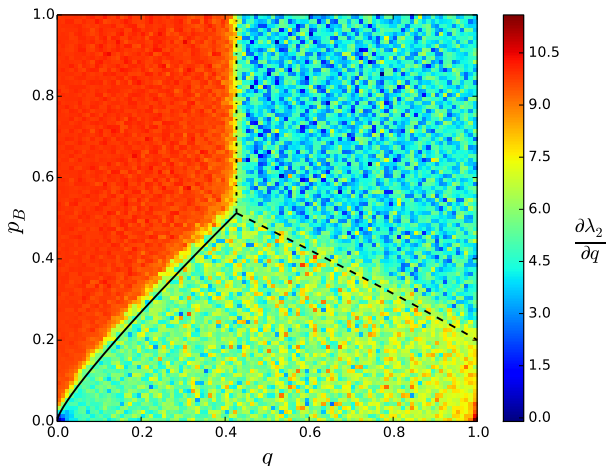


Figure 10: Heat-map of $\partial\lambda_2(\mathcal{L})/\partial q$ for two interacting Erdős-Rényi graphs of $N = 600$, $p_A = 0.5$, $M = 400$ and varying p_B . The three phases are delimited by the curve of eq. (2.16) with $p = p_B$ (solid line) and with $p = p_A$ (dashed-dotted line), plus the curve of eq. (2.18) (dashed line). Indeed, for $p_B \gtrsim 0.51(7)$ we are in the case $\lambda_2(\mathcal{L}_A)/N < \lambda_2(\mathcal{L}_B)/M$, hence there is only one transition at $q_c = \lambda_2(\mathcal{L}_A)/N \simeq 0.402(5)$. Instead for $p_B \lesssim 0.51(7)$ the first transition lies at $q_c = \lambda_2(\mathcal{L}_B)/M$, and the second one at $q'_c = [\lambda_2(\mathcal{L}_A) - \lambda_2(\mathcal{L}_B)]/(N - M)$ as long as $p_B \gtrsim 0.19(5)$. The triple point lies at $q_t = \lambda_2(\mathcal{L}_A)/N = \lambda_2(\mathcal{L}_B)/M$.

two transitions are observed at $q_c \simeq p_B$ and $q'_c \simeq (p_A - rp_B)(1 - r)$, provided $q'_c < 1$. The triple point obtains at $p_A = p_B = q$, *i.e.*, when the whole system is homogeneous.

The double transition of the algebraic connectivity described above is extremely important in the context of diffusion processes, since, as we mentioned in the Introduction, $\lambda_2^{-1}(\mathcal{L})$ is equal to the *relaxation time* τ for the diffusion equation $\dot{\mathbf{x}} = -\mathcal{L}\mathbf{x}$ (DLR15; MPL17). In the regime of small q , diffusion on the system depends only on the interconnection structure. The first transition occurs when the layer with the smallest normalized algebraic connectivity (be it $\lambda_2(A)/N$ or $\lambda_2(B)/M$) starts determining the diffusion process. The second transition then occurs when

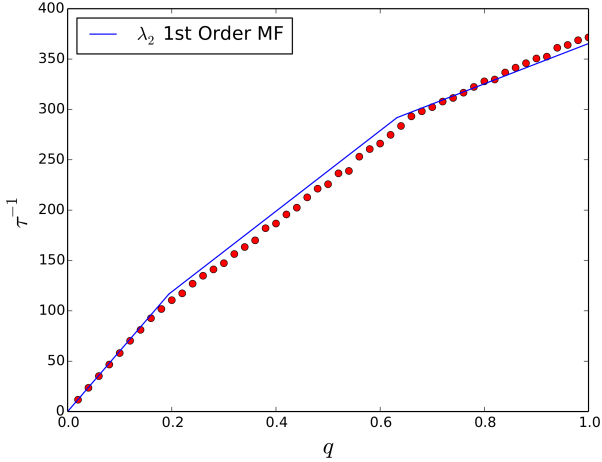


Figure 11: Inverse relaxation time τ^{-1} for the diffusion process $\dot{\mathbf{x}} = -\mathcal{L}\mathbf{x}$ on two Erdős-Rényi randomly interconnected networks with $N = 450$, $p_A = 0.45$, $M = 300$, $p_B = 0.3$ and varying q . Red points refer to numerical simulations, whereas, the blue solid line indicates the first order mean field approximation of $\lambda_2(\mathcal{L})$ of eq. (2.15).

the other layer becomes dominant, and can be observed because the two algebraic connectivities grow at different rates ($N \neq M$) as q increases. Note that the system becomes completely homogeneous only at the triple point q_t , when neither A nor B nor interconnections are dominant. Figure 11 shows that values of τ^{-1} obtained from numerical simulations of such diffusion processes on random interacting networks do agree well with first order mean field approximation of λ_2 .

2.3 Perturbative approach for the spectrum of the adjacency matrix

Perturbation theory can successfully be applied also in the computation of the leading eigenvalue of the supra-adjacency matrix \mathcal{C} of two interacting networks. Again we can interpret \mathcal{C} as the sum of an unperturbed

part and a perturbation

$$C = C_0 + \mathcal{W} = \begin{pmatrix} \mathcal{A} & 0 \\ 0 & \mathcal{B} \end{pmatrix} + \begin{pmatrix} 0 & \mathcal{Q} \\ \mathcal{Q}^\top & 0 \end{pmatrix}, \quad (2.19)$$

where \mathcal{A} and \mathcal{B} are the adjacency matrices of the two layers and \mathcal{Q} is the adjacency matrix of the inteconnections. We denote by $\{\alpha_i\}_{i=1}^N$ and $\{|a_i\rangle\}_{i=1}^N$ the set of eigenvalues and eigenvectors of \mathcal{A} , ordered such that $\alpha_1 > \alpha_2 \geq \dots \geq \alpha_N$, and by $\{\beta_j\}_{j=1}^M$ and $\{|b_j\rangle\}_{j=1}^M$ the set of eigenvalues and eigenvectors of \mathcal{B} , again ordered such that $\beta_1 > \beta_2 \geq \dots \geq \beta_M$. We assume both networks to be strongly connected, so that both α_1 and β_1 are not degenerate in their respective spectrum. We also suppose, without loss of generality, $\alpha_1 \geq \beta_1$. The sets

$$\{\Gamma_c^{(0)}\}_{c=1}^{N+M} = \{\{\alpha_i\}_{i=1}^N, \{\beta_j\}_{j=1}^M\}$$

and

$$\{|c^{(0)}\rangle\}_{c=1}^{N+M} = \left\{ \left\{ \begin{pmatrix} |a_i\rangle \\ |0\rangle \end{pmatrix} \right\}_{i=1}^N, \left\{ \begin{pmatrix} |0\rangle \\ |b_j\rangle \end{pmatrix} \right\}_{j=1}^M \right\}$$

are thus the unperturbed spectrum of eigenvalues and its associated orthonormal basis of eigenvectors for C_0 .

If $\alpha_1 = \beta_1$, we need to resolve the degeneracy with the unperturbed eigenstates $|+\rangle^{(0)} = \frac{1}{\sqrt{2}} \begin{pmatrix} |a_1\rangle \\ |b_1\rangle \end{pmatrix}$ and $|-\rangle^{(0)} = \frac{1}{\sqrt{2}} \begin{pmatrix} |a_1\rangle \\ -|b_1\rangle \end{pmatrix}$. We have

$$\langle +\rangle^{(0)} | \mathcal{W} | -\rangle^{(0)} = \langle -\rangle^{(0)} | \mathcal{W} | +\rangle^{(0)} = 0,$$

and:

$$\gamma_+^{(1)} = \langle +\rangle^{(0)} | \mathcal{W} | +\rangle^{(0)} = \langle a_1 | \mathcal{Q} | b_1 \rangle, \quad (2.20)$$

$$\gamma_-^{(1)} = \langle -\rangle^{(0)} | \mathcal{W} | -\rangle^{(0)} = -\langle a_1 | \mathcal{Q} | b_1 \rangle. \quad (2.21)$$

On the other hand there is no degeneracy when $\alpha_1 > \beta_1$. In this case, however, first-order corrections to all eigenvalues induced by the perturbation vanish since the interaction matrix \mathcal{Q} is different from 0 only in its off-diagonal blocks, therefore:

$$\gamma_c^{(1)} = \langle c^{(0)} | \mathcal{W} | c^{(0)} \rangle = 0. \quad (2.22)$$

Hence we have to resort to second-order corrections (see Appendix A). For α_1 we have:

$$\gamma_1^{(2)} = \sum_{j=1}^M \frac{|\langle a_1 | \mathcal{Q} | b_j \rangle|^2}{\alpha_1 - \beta_j}, \quad (2.23)$$

where we used $\langle b_j | \mathcal{Q}^\top | a_i \rangle = \langle a_i | \mathcal{Q} | b_j \rangle \forall i, j$. If also β_1 is non degenerate, then

$$\gamma_{N+1}^{(2)} = \sum_{i=1}^N \frac{|\langle a_i | \mathcal{Q} | b_1 \rangle|^2}{\beta_1 - \alpha_i}. \quad (2.24)$$

It turns out, however, that second-order corrections fail to capture the behavior of Γ_1 (see Figure 12). In order to obtain a non-vanishing first-order correction, we have to define the unperturbed system and the perturbation as

$$\mathcal{C} = \tilde{\mathcal{C}}_0 + \tilde{\mathcal{W}} = \begin{pmatrix} \mathcal{A} & 0 \\ 0 & \mathcal{B} + \Delta \mathcal{I} \end{pmatrix} + \begin{pmatrix} 0 & \mathcal{Q} \\ \mathcal{Q}^\top & -\Delta \mathcal{I} \end{pmatrix}, \quad (2.25)$$

where $\Delta = \alpha_1 - \beta_1$: we shift the whole unperturbed spectrum of \mathcal{B} by Δ , so that α_1 is now a degenerate eigenvalue for $\tilde{\mathcal{C}}_0$ with respect to the same eigenvectors $|a_1\rangle$ and $|b_1\rangle$. Using the same unperturbed eigenstates $|+^{(0)}\rangle$ and $|-^{(0)}\rangle$ as above, we obtain $\langle +^{(0)} | \tilde{\mathcal{W}} | -^{(0)} \rangle = \langle -^{(0)} | \tilde{\mathcal{W}} | +^{(0)} \rangle = \Delta/2$, $\langle +^{(0)} | \tilde{\mathcal{W}} | +^{(0)} \rangle = \langle a_1 | \mathcal{Q} | b_1 \rangle - \Delta/2$ and $\langle -^{(0)} | \tilde{\mathcal{W}} | -^{(0)} \rangle = -\langle a_1 | \mathcal{Q} | b_1 \rangle - \Delta/2$, that is a non-diagonal projection of $\tilde{\mathcal{W}}$ on the degenerate eigenspace spanned by $|+^{(0)}\rangle$ and $|-^{(0)}\rangle$. Therefore we need to solve the secular equation with respect to the unknown first order correction $\tilde{\gamma}^{(1)}$:

$$\det \begin{pmatrix} \langle +^{(0)} | \tilde{\mathcal{W}} | +^{(0)} \rangle - \tilde{\gamma}^{(1)} & \langle +^{(0)} | \tilde{\mathcal{W}} | -^{(0)} \rangle \\ \langle -^{(0)} | \tilde{\mathcal{W}} | +^{(0)} \rangle & \langle -^{(0)} | \tilde{\mathcal{W}} | -^{(0)} \rangle - \tilde{\gamma}^{(1)} \end{pmatrix} = 0, \quad (2.26)$$

which yields:

$$\tilde{\gamma}_{\pm}^{(1)} = -\frac{\Delta}{2} \pm \sqrt{\frac{\Delta^2}{4} + [\langle a_1 | \mathcal{Q} | b_1 \rangle]^2}. \quad (2.27)$$

Eq. (2.27) correctly reduces to eq. (2.20) if $\Delta = 0$, and to $\tilde{\gamma}_+^{(1)} = 0$ and $\tilde{\gamma}_-^{(1)} = -\Delta$ if \mathcal{Q} vanishes (which is trivially correct).

All of the above formulas can be further specified for simple instances of the interaction matrix. For a multiplex network, $N = M$ and $\mathcal{Q} = q\mathcal{I}$,

hence:

$$\langle a_i | \mathcal{Q} | b_j \rangle = q \langle a_i | b_j \rangle. \quad (2.28)$$

Instead for two randomly interacting networks, \mathcal{Q} is an Erdős-Rényi random graph with connectivity q . Using the mean field approximation $\mathcal{Q} = q |1\rangle \langle 1|$ leads to:

$$\langle a_i | \mathcal{Q} | b_j \rangle = q \langle a_i | 1 \rangle \langle 1 | b_j \rangle. \quad (2.29)$$

2.3.1 Random regular and Erdős-Rényi network layers

More can be said when both \mathcal{A} and \mathcal{B} are d -regular graphs. In this case, it is $\alpha_1 = d_A$, $|a_1\rangle = \frac{1}{\sqrt{N}} |1\rangle$, $\beta_1 = d_B$, $|b_1\rangle = \frac{1}{\sqrt{M}} |1\rangle$. Besides, for sufficiently large network sizes, most d -regular graphs have all their other eigenvalues bounded above by $2\sqrt{d-1} + \varepsilon$ (with $\varepsilon > 0$) (Fri03). Thus, provided $d_B \gg 2\sqrt{d_A-1}$, α_1 and β_1 are by far the largest eigenvalues of the unperturbed system. Finally, eigenvectors corresponding to other eigenvalues are orthogonal to $|1\rangle$, hence $\langle 1 | a_i \rangle = \langle 1 | b_j \rangle = 0$ for $i \neq 1$ and $j \neq 1$.

Thus in a multiplex framework where $N = M$ it is $|a_1\rangle \equiv |b_1\rangle$. Using eq. (2.28) and the eigenvectors orthogonality relations, we have $\langle a_1 | \mathcal{Q} | b_j \rangle = q\delta_{1j}$ and $\langle a_i | \mathcal{Q} | b_1 \rangle = q\delta_{i1}$. In the degenerate case we get $\gamma_{\pm}^{(1)} = \pm q$, whereas, in the non-degenerate case it is $\tilde{\gamma}_{\pm}^{(1)} = -\Delta/2 \pm \sqrt{\Delta^2/4 + q^2}$ and $\gamma_1^{(2)} = q^2/(\alpha_1 - \beta_1) = -\gamma_{N+1}^{(2)}$.

In the random interaction framework instead, using eq. (2.29) and again the eigenvectors orthogonality relations, we have $\langle a_1 | \mathcal{Q} | b_j \rangle = q\sqrt{NM}\delta_{1j}$ and $\langle a_i | \mathcal{Q} | b_1 \rangle = q\sqrt{NM}\delta_{i1}$. In the degenerate case we get $\gamma_{\pm}^{(1)} = \pm q\sqrt{NM}$, and in the non-degenerate one $\tilde{\gamma}_{\pm}^{(1)} = -\Delta/2 \pm \sqrt{\Delta^2/4 + q^2NM}$ and $\gamma_1^{(2)} = q^2NM/(\alpha_1 - \beta_1) = -\gamma_{N+1}^{(2)}$.

Finally note that a d -regular graph of size N is, under the mean field approximation, equivalent to an Erdős-Rényi random graph with same size and connectivity $p = d/(N-1)$. Hence, the above results approximately hold also for \mathcal{A} and \mathcal{B} being Erdős-Rényi random graphs, in particular by posing $\alpha_1 = p_A(N-1)$ and $\beta_1 = p_B(M-1)$ (see Fig. 12).

This approach can be rather useful for estimating the bond percolation threshold f_c of two strongly interacting random networks, where

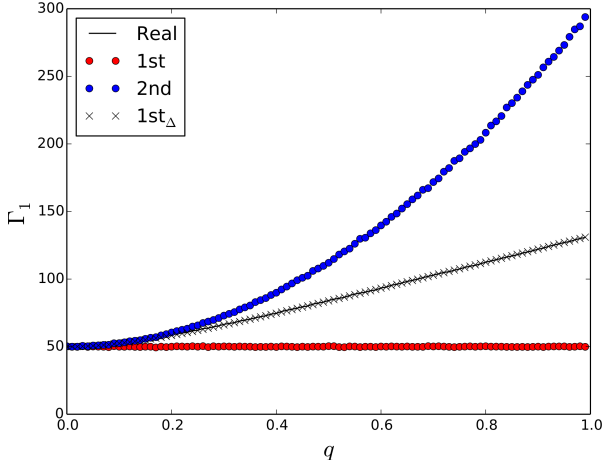


Figure 12: Largest eigenvalue of \mathcal{C} as a function of q for two interacting Erdős-Rényi graphs of $N = M = 100$, $p_A = 0.5$ and $p_B = 0.1$, together with first-order corrections of eq. (2.22), second-order corrections of eq. (2.23), and first-order corrections of eq. (2.27).

the magnitude of the interaction is given by the value of q . As a matter of fact when the value of q is small enough the two layers are in a regime of weak interaction, therefore two percolation thresholds associated to different second-order phase transitions may be observed depending on the different topologies of the two layers (HCG⁺16)(CdSBn14). However very weak interaction between layers can also induce abrupt transitions in the order parameter, therefore second-order phase transition theory does not apply: we are going to provide a detailed explanation of this phenomenon in the next chapter.

On the other hand, while for an individual Erdős-Rényi network layer f_c is given by the inverse of the largest eigenvalue of adjacency matrix Γ_1 (BBCR10a) (or in general is lower-bounded by Γ_1^{-1} (RC16a)), Figure 13 shows that for two strongly interacting layers, where q is not negligible, the percolation threshold is actually determined by eq. (2.27).

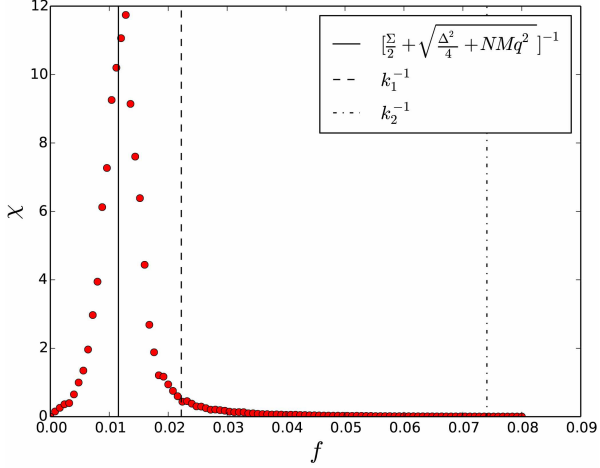


Figure 13: Numerical value of the susceptibility χ as a function of the bond occupation probability f for 400 realizations of the process on two random ER interacting networks with $N = 150$, $p_A = 0.1$, $M = 100$, $p_B = 0.5$ and $q = 0.5$. The solid black line denotes the mean field first-order correction to Γ_1^{-1} of eq. (2.27), whereas, the dashed and dashed-dotted lines denote the percolation thresholds of individual layers $k_1^{-1} = (Mp_B)^{-1}$ and $k_2^{-1} = (Np_A)^{-1}$. It is $\Sigma = k_1 + k_2$ and $\Delta = k_1 - k_2$.

Chapter 3

Fragility and anomalous susceptibility of weakly interacting networks

3.1 Percolation in multilayer networks

Multilayer networks have been shown to exhibit critical percolation properties which are different from what is observed for a single isolated network—namely, a single continuous phase transition (CNSW00; NSW01) whose properties depend on the kind of process (RC15a) and on the network features (CbAH02a; CPS10). Indeed, the presence of interconnections between the network layers can give rise to supercritical phenomena such as abrupt or multiple phase transitions.

For instance interdependent networks—that is, two (or more) networks whose nodes are interconnected by dependency links, such that the removal of a node in a network causes the instantaneous removal of the dependent nodes in the other networks—have a discontinuous percolation transition (BPP⁺10; GBHS11; PBH11; SBC⁺12; BDGM12). Further introducing interdependence probabilities (meaning that only some of the dependency links actually exist), multiple percolation phase transitions can occur in these systems (BD14), whereas, introducing redun-

dant interdependencies among layers boosts the robustness of the system (RB17). For “weak” interdependence, *i.e.*, a finite probability that a node is not removed when its dependent neighbours are, mixed percolation transitions are observed, for which each network layer undergoes its own distinct transition (either discontinuous or continuous) (LESL18). And when interdependent networks are enriched with antagonistic interactions, which prevent antagonist nodes to be part of the same percolation cluster, the percolation process can become bistable, meaning that either of the two networks is allowed to percolate (ZB13a; ZB13b). Note that the sharp transition usually observed in interdependent networks is actually smoothed (and eventually goes back to being continuous) by the presence of link overlaps between the various layers (LLJW13; CLZ⁺13; HZZ⁺13). Assortative correlations in particular lead to recurrent hybrid phase transitions (BBdC⁺16; LCS⁺16). On the contrary, the presence of highly anti-correlated layers lead to multiple transitions indicating that each layer can percolate independently (HCG⁺16).

Interacting networks (or network of networks) are different from interdependent networks in that the connections between the network layers are ordinary links that thus take part in the percolation process. A system of this kind is therefore equivalent to a single modular network, characterised by a percolation threshold that is typically lower than in homogeneous networks—with a giant cluster appearing for a smaller total number of links (LD09). A case of particular interest arises when the interaction between the network layers is weak, meaning that there is a sufficiently small number of interlinks between network layers, so that the removal of a few of them can easily separate the network layers into isolated modules (SKK⁺15). This setup is common for neural systems, and therefore of major relevance to understand the resilience of neural processing (HI97). Weakly interacting networks are characterised by a mixed percolation phase, in which only one or some of the network layers do percolate (DHS12; MPMG14). In particular, Colomer-de-Simón & Boguñá (CdSBn14) identified multiple percolation transitions when the coupling between the different layers vanishes in the thermodynamic limit. In order to account for the emergence of coexisting percolating

clusters, Faqeeh *et al.* (FMCdSG16) developed a modular message passing approach. In any event, the appearance of these coexisting clusters in weakly interacting networks is a fundamental source of error for percolation theory.

In what follows we develop a simple mathematical framework that allows estimating the most likely critical threshold at which the merging of coexisting clusters occurs in weakly interacting networks. Moreover, we characterise the percolation process in terms of a powder keg: due to the scarcity of the interlinks, the aggregation of the coexisting giant clusters is delayed, therefore giving rise to an abrupt percolation transition.

3.2 The intrinsic powder keg of weakly interacting networks

To illustrate the percolation properties of weakly interacting networks, we consider as in Figure 14 two layers A (with N_A nodes and average degree k_A) and B (with N_B nodes and average degree k_B), that are interconnected by a small number I of links ($I \ll \min\{N_A k_A, N_B k_B\}$)¹. The bond percolation process consists in retaining each link of the system with occupation probability f and otherwise removing it. To simulate the process, we use the method proposed by Newman and Ziff (NZ00a): for each realisation, we start from a system configuration with no connections, and then sequentially add links in a random order. f is thus the fraction of links added to the system. In such a situation, we may observe large jumps for the order parameter S , that is, the size of the giant cluster spanning both layers. These jumps can be understood as resulting from the addition of one of the I interlinks *after* the formation of the two giant clusters S_A and S_B of layer A and B , respectively. Indeed, differently from what happens for standard percolation, when such interlink is about to be added the two giant clusters already contain a number of nodes that is proportional to the system size. According to

¹For the sake of readability here we decided to adopt a different notation for layers sizes compared to the one used in the previous chapter, hence layers sizes here are denoted as N_A, N_B instead of N, M .

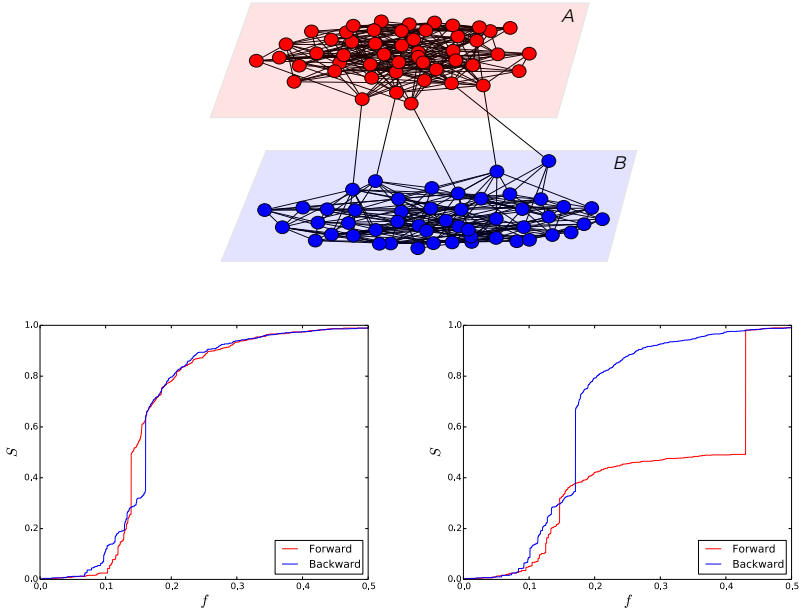


Figure 14: Upper panel: pictorial representation of two weakly interacting networks A and B , in which the interconnection links I are much less than the intra-layer links. Lower panel: two different instances of the percolation process on an interacting network composed by two Erdős-Rényi layers ($N = 500$ nodes and average degree $k = 10$ each) connected by $I = 5$ interconnection links. Each realisation is obtained as follows. Starting from an empty network, links are first randomly added (*forward*) up to half the total number of links, and then randomly removed (*backward*) until the network is empty again. The hysteresis cycle appearing in both cases are remarkably different, because of the large variability of the percolation threshold.

the definition of Friedman *et al.* (FL09), this configuration corresponds to a *powder keg*, which is “ignited” as soon as that interconnection is added causing a discontinuous jump in the size of the giant component. Note that if a system is initialised as a powder keg, then even a random link addition rule causes a discontinuous transition: as in our case, the formation of the giant cluster spanning both layers is not hindered by specific link selection rules (ADS09; GCB⁺11; NLT11; NTG12; DN15), but is naturally delayed by the structure of the interconnections itself. However, the absence of any particular link selection criterion causes a large uncertainty for the abrupt percolation threshold (see fig. 14). Note that since the process of adding links is arbitrary, the probability to activate one of the I interconnection links *before* the formation of the two giant cluster is a non vanishing quantity: in this particular case we do not expect to observe a significant jump for S . To work out a rough estimate for this phenomenon let us define as Π_τ the probability that at discrete time τ (hence after the random addition of τ links) none of the I interconnection links has been yet activated. For sake of simplicity let us consider the two layers to be characterised by the same percolation threshold f_c and let E be the total number of edges. It is then possible to write:

$$\Pi_\tau = \left(1 - \frac{I}{E}\right) \left(1 - \frac{I}{E-1}\right) \dots \left(1 - \frac{I}{E-\tau+1}\right) = \frac{\binom{E-\tau}{I}}{\binom{E}{I}}, \quad (3.1)$$

which in the case of weak interaction and small times (hence $I \ll \{E, E-\tau\}$) can be approximated as

$$\Pi_\tau \cong \frac{(E-\tau)^I}{E^I} = \left(1 - \frac{\tau}{E}\right)^I. \quad (3.2)$$

Note that in general we can express f_c as a critical edge density to be achieved at a critical time τ_c , hence $f_c = \tau_c/E$. By plugging the latter in eq. (3.2) we obtain:

$$\Pi_{\tau_c} \cong (1 - f_c)^I. \quad (3.3)$$

In figure (14) we considered two Erdős-Rényi layers of 500 nodes each with same average connectivity $k = 10$ (therefore $f_c \simeq 1/k = 0.1$ for each layer), connected by $I = 5$ interconnection links. The approximation of

eq. (3.3) then tells us that $\Pi_{\tau_c} \sim 0.6$ for this case, meaning that a significant discontinuous jump would reasonably be unlikely to be observed in the 40% of the cases. However with this very rough approximation we are neglecting the fact that, in order to observe a discontinuous jump in S , a randomly added interconnection link must also connect two nodes which belong to the percolating clusters of the two layers.

3.3 Model for the anomalous susceptibility and percolation threshold

In order to gain a more quantitative insight on the described phenomenology, we define the probability P_I that at least one of the I interconnections is added and actually connects the two giant clusters S_A and S_B (FMCdSG16):

$$P_I = 1 - \left[1 - \left(\frac{N}{N_A} S_A \right) \left(\frac{N}{N_B} S_B \right) f \right]^I = 1 - \left[1 - \frac{N}{\mu} S_A S_B f \right]^I, \quad (3.4)$$

where $N = N_A + N_B$ is the total number of nodes, the normalisation coefficients before S_A and S_B respectively denote their maximum size N_A/N and N_B/N , and $\mu = \frac{N_A N_B}{N_A + N_B}$ is the *reduced* number of nodes (equivalently to the concept of reduced mass for the classical two-body problem)². Without loss of generality, we set the percolating thresholds f_A and f_B of the individual layers A and B respectively such that $f_A < f_B$ (the degenerate case $f_A = f_B$ is discussed below). This implies that on average and for layers of the same nature we have $S_A > S_B$ for any given value of f such that both clusters exist. Hence, for $f > f_B$, the percolation cluster S of the whole system is either that of layer A if S_A and S_B are not connected, or abruptly jumps to $S_A + S_B$ provided that S_A and S_B are connected—which happens with probability P_I . In formulas,

$$S = \begin{cases} S_A + S_B & \text{with probability } P_I \\ S_A & \text{otherwise} \end{cases} \quad (3.5)$$

² Note that in the case $N_A = N_B$, if we assume that almost every node belongs to the percolating cluster of A or B (hence $S_A = S_B \sim 1/2$) we correctly obtain $P_I(f_c) = 1 - \Pi_{\tau_c}$ according to the approximation of eq. (3.3).

Overall, we have a first continuous transition at $f_1 = f_A$ (the standard percolation transition when layer A percolates), and a second discontinuous transition at f_2 when layer B percolates and at least one active interconnection is established between the two layers. Yet, because of the dichotomy characterising the outcome of the process for $f \simeq f_2$, the average value $\langle S \rangle = S_A + S_B P_I$ is not representative at all of what happens in the system. We thus study the behaviour of the susceptibility $\chi = N \text{Var}(S) / \langle S \rangle$ (CdSBn14). For $f > f_B$ each layer has its own percolating cluster, and thus the only contribution to χ comes from the Bernoulli trial described by eq. (3.5):

$$\chi_D = N \frac{S_B^2 P_I (1 - P_I)}{S_A + S_B P_I}. \quad (3.6)$$

Note that χ_D gives a non-vanishing contribution to the total susceptibility χ only in the weakly interacting regime, that is, when the Bernoulli trial of eq. (3.5) is not trivial. Indeed, eq. (3.4) tells us that for $I \rightarrow 0$ (as for the case of disconnected layers) we have $P_I \rightarrow 0$, and when I is very large (as is the case of strongly connected layers, see section below) we have $P_I \rightarrow 1$. In both cases $\chi_D \rightarrow 0$. For fixed I , however, χ_D achieves its maximum for the value of f which maximises the uncertainty of the Bernoulli trial, at which the discontinuous jump of S is more likely to occur. We thus identify f_2 with the value for f which maximises χ_D .

3.4 Real and artificial networks

These simple mathematical arguments are indeed able to capture the behaviour of the susceptibility both in real and model networks. We first consider in Figure (15) the duplex (two-layer multiplex) formed by a pair of coupled air transportation networks, where each layer consists of the airports (nodes) and flight routes (links) operated by a given company, and the interlinks are the airports served by both companies. We see that the susceptibility of the two individual layers χ_C cannot capture the observed behaviour of χ computed numerically. The difference between χ and χ_C is instead very well represented by χ_D . In particular, from figure (15b) we can see that χ_D can give a dominant contribution to the

whole susceptibility χ . In this case standard methods for the estimation of the percolation threshold (such as looking at the inverse of the leading eigenvalue of the Hashimoto non-backtracking matrix (KNZ14a)) fail significantly.

A more precise assessment of our methodology is given by considering two Erdős-Rényi weakly interacting networks with the same number of nodes $N_A = N_B = N/2$ and average degrees k_A and k_B . We start from the implicit form of S_A and S_B in the thermodynamic limit:

$$S_X = \frac{1}{2} (1 - e^{-2fk_X S_X}) \quad (3.7)$$

with $X = \{A, B\}$. The above expression is obtained from the usual equation for a single Erdős-Rényi network, namely $S = 1 - e^{-f k S}$, using the substitution $S \rightarrow 2S$ (as S_X refers to only one layer with half of the N nodes). We thus obtain the same solution of the single network scaled by a factor $1/2$, as well as the same percolation threshold $f_X = k_X^{-1}$. The value of f which maximises χ_D of eq. (3.6) for fixed S_A and S_B is given by the following implicit equation

$$[1 - 4f_2 S_A S_B]^I = 1 + \frac{S_A - \sqrt{S_A^2 + S_A S_B}}{S_B}, \quad (3.8)$$

where both S_A and S_B are functions of f_2 according to eq. (3.7). Note that eq. (3.8) returns $f_2 = 1 - (2 - \sqrt{2})^{1/I}$ in the limit $S_{A,B} \rightarrow 1/2$. This regime corresponds to the case $I \ll k_{A,B}$, for which we can safely assume that both layers will fully percolate before the activation of at least one interconnection link as f increases, leading to a value of f_2 which does not depend on k_A nor k_B . Since eq. (3.8) is difficult to handle, we can approximate f_2 with the values that maximises $\text{Var}(S)$ instead of χ_D . For a Bernoulli trial we simply have $P_I(f_2) = 1/2$, implying $f_2 = [1 - 2^{-1/I}]/[4S_A S_B]$. With the further assumption $S_A \simeq 1/2$ (hence when layer A has already percolated) we have $f_2 = [1 - 2^{-1/I}]/[2S_B]$. Using eq. (3.7) we finally get the analytic solution:

$$f_2 = \frac{1 - 2^{-1/I}}{1 - \exp[-k_B(1 - 2^{-1/I})]}. \quad (3.9)$$

In the limit $S_B \rightarrow 1/2$ this expression simplifies to $f_2 = 1 - 2^{-1/I}$, which

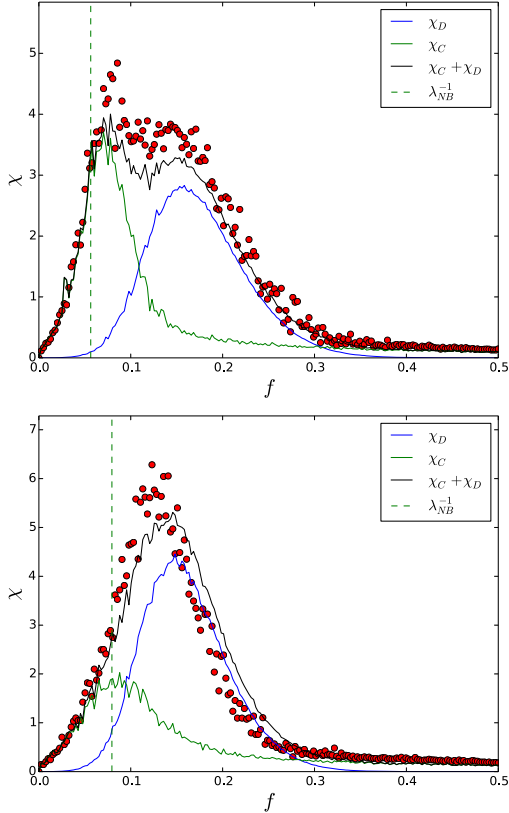


Figure 15: We consider the duplex formed by the transportation network Lufthansa-Ryanair (upper panel) and Lufthansa-Easyjet (lower panel) (CGGZ⁺13), in which each layer is made up of airports (nodes) and flight routes (links) operated by a company. The layers are characterised by $N_{LH} = 106$ and $\langle k \rangle_{LH} = 4.604$, $N_{FR} = 128$ and $\langle k \rangle_{FR} = 9.391$, $N_{U2} = 99$ and $\langle k \rangle_{U2} = 6.202$. The interconnection links in each case are the airports in which both companies operate: we have $I_{LH-FR} = 36$ and $I_{LH-U2} = 51$. Red dots denote numerically computed values of χ from 400 realisations of the bond percolation process, χ_D is given by eq. (3.6) and χ_C is the susceptibility of the corresponding non-interacting system. λ_{NB} is the leading eigenvalue of the non-backtracking matrix of the network, whose inverse is a good approximation for the percolation threshold of sparse networks (KNZ14a).

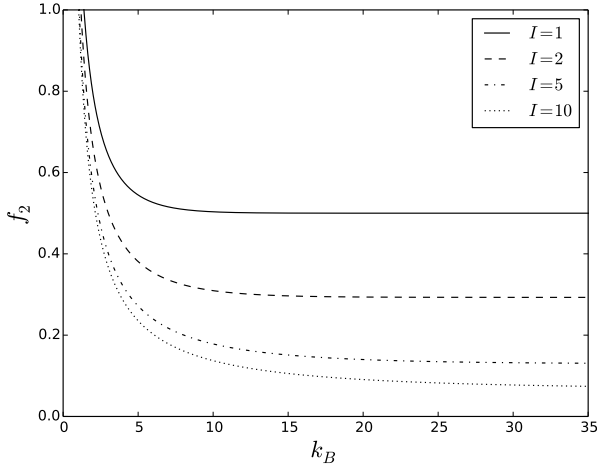


Figure 16: Plot of eq. (3.9) for 4 different values of I and $k_B = 20$.

is very close to the value that maximises χ_D in the same regime. Figure (16) shows the plot of f_2 for different values of I .

In the degenerate case $k_A = k_B = k$, we have $S_A = S_B = S_X$ which leads to the simpler expressions:

$$\langle S \rangle = S_X(1 + P_I), \quad \chi_D = N \frac{S_X P_I (1 - P_I)}{1 + P_I}, \quad (3.10)$$

and thus the value of f which maximises χ_D at fixed S_X is simply given by the implicit expression $P_I(f_2) = \sqrt{2} - 1$, implying $f_2 = [1 - (2 - \sqrt{2})^{1/I}] / [4S^2]$. Plugging the latter in eq. (3.7) yields

$$f_2 = \frac{1 - (2 - \sqrt{2})^{1/I}}{\left\{ 1 - \exp \left[-k \sqrt{f_2} (1 - (2 - \sqrt{2})^{1/I}) \right] \right\}^2}, \quad (3.11)$$

that can be easily solved numerically.

As shown in Figure 17, in the case of two weakly interacting Erdős-Rényi networks with different average degrees, the numerical evaluation of

χ_D by means of eq. (3.6) fits very well the observed anomalous susceptibility, and the numerical solution of eq. (3.9) gives with good approximation the position of the maximum of χ . In the degenerate case $k_A = k_B$, eq. (3.11) provides an even better approximation for the maximum of χ . Analysing single realisation of the percolation process, we confirm that f_2 marks the region in which S is subject to discontinuous jumps. However, this discontinuous behaviour is lost by averaging the outcomes of the percolation process over many realisations, for which S becomes $\langle S \rangle = S_A + P_I S_B$ which fails to represent the outcome of the process.

3.5 Finite size scaling

A finite-size scaling analysis was carried out for the cases of two coupled Erdős-Rényi layers and two coupled Barabási-Albert layers with different average connectivities. For each of the two settings we considered networks made of two layers of size $N_{A,B}$ equal to 100, 500, 2500, 12500. According to standard percolation theory, the maximum of the susceptibility diverges around the critical value f_c according to the power law $\chi(f_c) \sim N^{1-\beta/\nu}$, while for the relative size of the giant component we have $S(f_c) \sim N^{-\beta/\nu}$ (CdSbn14; RC15a). Our analysis, reported in Figure 18, shows that the scaling properties around f_1 and f_2 are significantly different. While $S(f_1)$ and $\chi(f_1)$ exhibit the usual power law scaling typical of second-order phase transitions (with different exponents according to the two different topologies of the network layers), $S(f_2)$ does not scale with N in both examples, which implies $\beta/\nu = 0$. This in turn implies $\chi(f_2) \sim N$. It is important here to give some further details on how the system has been scaled. In (CdSbn14) the existence of a double percolation transition was verified under the assumptions of both constant core/periphery average degree and sub-linear scaling of the total number of core-periphery interconnections (yielding a vanishing average core-periphery degree), which translates as $I \propto N^\alpha$, with $0 \leq \alpha < 1$. All the numerical results presented here above were obtained in the case of constant $k_{A,B}$ and I , hence in the case $\alpha = 0$. This particular choice has

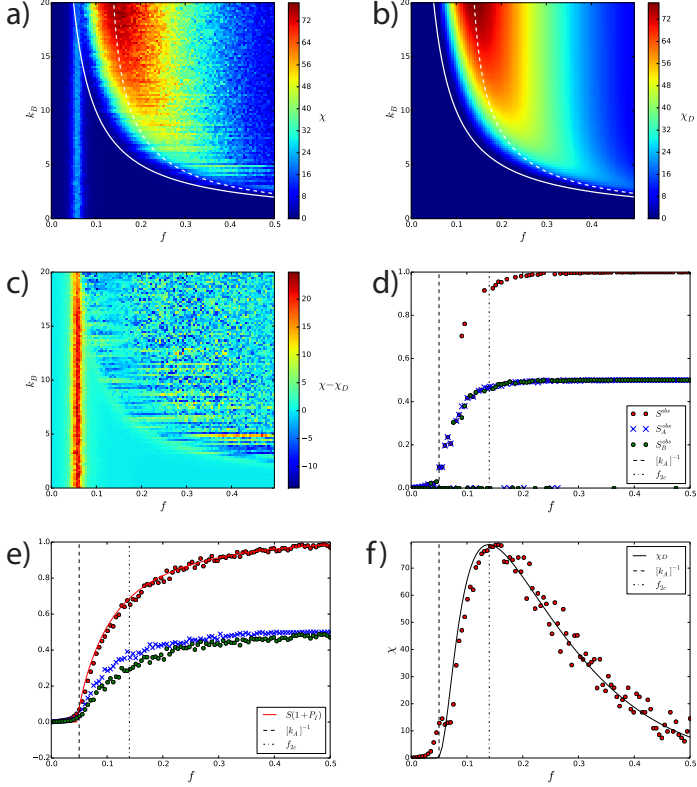


Figure 17: Panels (a-c) are heat maps of the susceptibility of two Erdős-Rényi coupled networks with $N_A = N_B = 500$ nodes, $k_A = 20$, $I = 5$ and k_B varying from 0 to k_A . Panel (a) reports χ obtained from numerical simulations of the percolation process, whereas, panel (b) reports χ_D from numerical solutions of eq. (3.6). In both cases, the continuous white line gives the relation $f = k_B^{-1}$ that marks the boundary for the region in which percolating clusters exist in both layers, and the dashed white line reports values of f_2 as given by eq. (3.9). Panel (c) reports the difference between the two values, which is high only in the vertical strip corresponding to χ_C . Panels (d-f) instead report S and χ for the degenerate case of two Erdős-Rényi interacting layers with $N_A = N_B = 500$ and $k_A = k_B = 20$, and $I = 5$. In all three cases, the dashed vertical line denotes the percolation threshold of the individual layers, whereas, the dashed-dotted line marks f_2 as derived from eq. (3.11). Panel (d) reports a single realisation of the process and Panel (e) reports averages of the same process over 300 realisations. In both cases, red dots are the observed values of S , blue crosses and green dots are the observed values of S_A and S_B respectively, and the red line gives the numerical estimate of $\langle S \rangle$ derived from eq. (3.5). Panel (f) finally reports the observed susceptibility (red dots) averaged over 300 realisations of the process, as well as the numerical value of χ_D (continuous black line).

been motivated by the fact that in our approximation regime f_2 is essentially a function of k_A, k_B, I (see section 3.4). Furthermore if we assume both layers to be particularly dense, the dependence from $k_{A,B}$ eventually disappears, hence the transition can be described only in terms of I , independently from the topologies of A and B . As a matter of fact in this rather extreme situation we can safely assume that both layers will percolate before the discontinuous transition, which implies $S_{A,B} \simeq 1/2$ at $f = f_2$. As discussed in section 3.4, in this case f_2 depends only on I . Overall from our results we can deduce that these particular scaling properties, that is the failure of finite size scaling relations ($\beta/\nu = 0$) and the extensive character of the susceptibility ($\chi(f_2) \sim N$), show a clear trademark of a first order phase transition (RF09). This fact essentially implies that on average the abrupt transition due to delayed aggregation of coexisting percolation clusters is discontinuous even in the thermodynamic limit.

3.6 Strongly Interacting Networks

To conclude we consider the case of strongly interacting Erdős-Rényi layers, that we define by $I \geq \max\{k_A, k_B\}$. As shown in Figure 19 (where $k_A > k_B$), as soon as $I > k_A$ the height of the second peak drastically decreases, while the corresponding value of f_2 approaches k_B^{-1} , that is, the percolation threshold of the sparser layer. As a matter of fact if we consider (3.9), the result is simply obtained thanks to the following first-order Taylor expansion:

$$f_2 = \frac{1 - 2^{-1/I}}{1 - \exp[-k_B(1 - 2^{-1/I})]} \xrightarrow{I \rightarrow \infty} \frac{1 - 2^{-1/I}}{1 - 1 + k_B(1 - 2^{-1/I})} = \frac{1}{k_B}.$$

Indeed when $I \rightarrow \infty$ we have $P_I \simeq 1$ as soon as the percolating cluster appears in layer B : the process bears no uncertainty related to the interconnections, therefore contribution of χ_D vanishes and χ simply becomes that of the ordinary percolation process for the Erdős-Rényi layer B .

Finally, if $I \gtrsim Nk_{A,B}$ then the total average degree is significantly af-

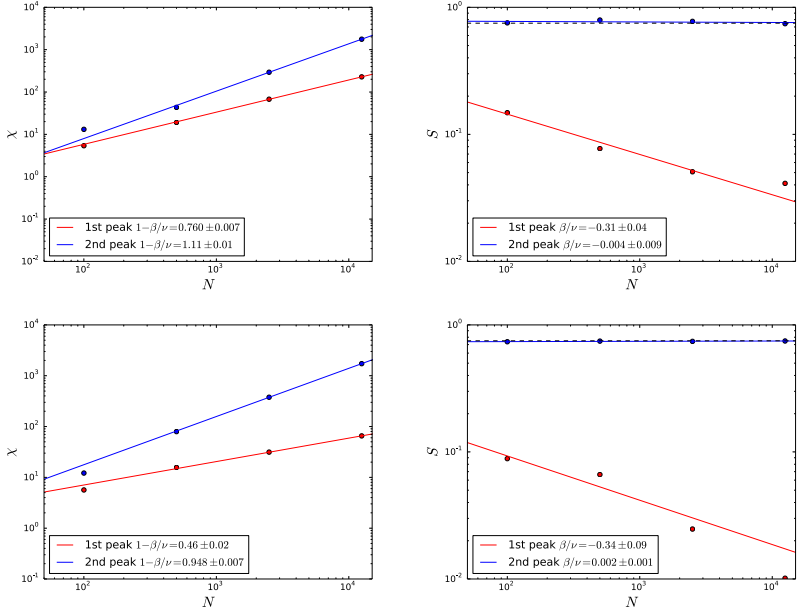


Figure 18: Finite size scaling analysis. Top panels report the case of two weakly interacting Erdős-Rényi layers with $k_A = 20$, $k_B = 10$ and $I = 5$, for different size N . From (b) we see that while $S(f_1)$ shows a power law decay with exponent $\beta/\nu = 0.31 \pm 0.04$ (which is consistent with the mean-field values $\beta = 1$ and $\nu = 3$), $S(f_2)$ does not scale with N . Accordingly to those values, from (a) we can verify the different divergence rates for the two peaks of the susceptibility, and in particular we see that the divergence of $\chi(f_2)$ is almost linear. Bottom panels instead report the case of two weakly interacting Barabási-Albert layers with $m_A = 20$, $m_B = 10$ and $I = 5$, for different size N . Again we see that while $S(f_1)$ and $\chi(f_1)$ show a scaling behaviour ruled by the topology of the layers, $S(f_2)$ and $\chi(f_2)$ show the same behaviour of the Erdős-Rényi case: the one characteristic of first-order phase transitions.

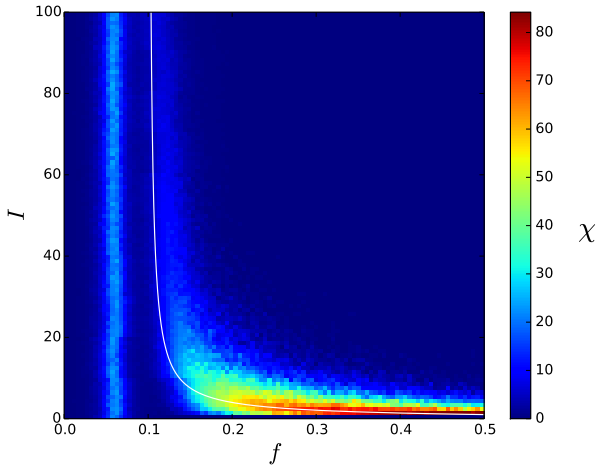


Figure 19: The case of strongly connected layers. Heatmap of the susceptibility χ for two Erdős-Rényi layers of $N = 500$ with $k_A = 20$, $k_B = 10$ and $0 < I < 100$. For every fixed value of I , χ is averaged over 400 realisations of the bond percolation process. The continuous white line represents the theoretical prediction from eq. (3.9), which for large values of I converges to $k_B^{-1} = 0.1$.

fected and we are in the regime illustrated in the previous chapter, that is the regime on which perturbation theory to the largest eigenvalue of the adjacency matrix may apply. Indeed, in this case we expect to see only one maximum in the susceptibility, since $\chi_D \cong 0$ and since I grows linearly with N (CdSBn14). We can therefore use the correction given by eq. (2.27) in order to estimate value of the single percolation threshold f_1 .

Chapter 4

Numerical Assessment of the percolation threshold using complement networks

Percolation properties in network models (be they sparse treelike graphs (CbAH02b) or clustered networks (SBn06; New09)) are often considerably different from those of real-world networks—which feature a highly more complex topology. Recently, percolation has been reformulated as a message passing process which takes as input the detailed topology of a given network to predict percolation-related observables (KNZ14b; HP14), and which implies that the bond percolation threshold π_c of the network is bounded from below by the leading eigenvalue of its non-backtracking matrix (HN14). This approach has been then generalized to clustered networks (RC16b), in order to go beyond the locally treelike approximation which is not reliable for networks with high density of edges and short loops (Rad15). However, the method comes at a price of much higher computational complexity, and is not particularly satisfactory for bond percolation processes. Another important aspect of the message passing approach is that it describes network percolation in the

thermodynamic limit, and as such cannot be precisely applied to finite graphs (TdCDM17). Indeed, the very percolation transition is ill defined in finite systems.

4.1 Numerical methods and preliminary results

Numerical simulations of the percolation process obtain the value of the percolation threshold p_c using Monte Carlo techniques (NZ00b). Given Q independent realizations of the process at fixed percolation probability p , and the relative size of the largest cluster in the network $s_q(p)$, $q = 1, \dots, Q$ in the q -th realization, the percolation strength at p is estimated as $S(p) = \frac{1}{Q} \sum_q s_q(p)$, and the susceptibility as $\chi(p) = \frac{1}{Q \cdot S(p)} \sum_q [s_q(p)]^2 - S(p)$. As we showed in the previous chapter, the best estimate of the percolation threshold is then the value of p at which the susceptibility is maximal. As the simulated system is finite, such defined pseudo-critical threshold $p_c(N)$ decays towards the percolation threshold as $p_c(N) - p_c \sim N^{-1/\nu}$, where N is the (finite) size of the network (RC15b).

Figure 20 shows, for the bond percolation problem, the relation between the value p_c obtained in numerical simulations and the theoretical π_c given by the inverse of the leading eigenvalue of the non-backtracking matrix (λ_{max}). The plot is obtained by considering a total of 79 networks of different sizes N (varying approximately from 20 to 890), 23 of which are empirical while the remaining 56 are artificially generated according to four different random network models: Erdős-Rényi (ER), Regular (RG), Barabási-Albert (BA) and Watts-Strogatz (SW) (New03). Points are well fitted by a linear relation $p_c = \pi_c/\beta$ with $\chi^2/\nu = 4.34$, where however the value of $\beta = 0.791 \pm 0.019$ is different from unity: numerical and theoretical percolation thresholds do not coincide, yet their ratio appears to be constant across a variety of empirical and model networks of different size. While assessing the general validity of such an empirical evidence needs further statistical analysis, this relation can be quite valuable for correcting the theoretical value of π_c for finite, non-treelike networks.

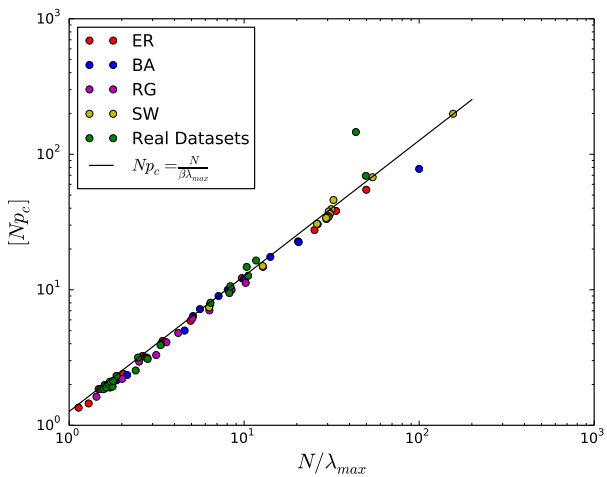


Figure 20: Plot of Np_c versus $N\pi_c = N/\lambda_{max}$, where λ_{max} is the leading eigenvalue of the non-backtracking matrix, for several model and empirical networks. Note that accounting for the factor N allows to compare networks of different size. The black solid line is the linear fit $p_c = \pi_c/\beta$.

4.2 Introduction of the complement graph and further results

Here we explore the possibility to improve such an empirical relation using the concept of *complement graph*. The complement of a graph G is the graph \bar{G} with the same vertex set, but whose edges are those which are not present in G (CE83; GY98). The union graph of G and \bar{G} is therefore a complete graph. Hence, if we indicate K as the adjacency of the complete graph and A as the adjacency matrix of G , the adjacency matrix of \bar{G} is simply defined as (see also Appendix B):

$$\bar{A}_{ij} = K_{ij} - A_{ij} = 1 - \delta_{ij} - A_{ij}, \quad (4.1)$$

where δ is the usual Kronecker delta. For further details about the properties of complement graphs see Appendix B.

Complement graphs are found since long in the mathematic literature, for instance to address the graph coloring problem (NG56), to develop graph compression schemes (KOT98) and search algorithms (IY98), to study network synchronizability (DLC08), to assess graph hyperbolicity (BRST11) and domination numbers (HW04). The common approach of these studies is to prove rigorous results for graphs with a small number of vertices (AH79; Xu87; PRS03). Here, for the first time to our knowledge, we use complement graphs in the context of percolation on large-scale complex networks. In particular, we investigate on the existence of a complement relation for the percolation threshold p_c of a given graph G and the complement percolation threshold \bar{p}_c of \bar{G} .

Now, since the complement of a sparse network is dense, in the thermodynamic limit the percolation threshold of \bar{G} converges to the inverse of the leading eigenvalue of the adjacency matrix of \bar{G} (BBCR10b). In the simple case of ER networks, for $N \rightarrow \infty$ it is $p_c \simeq 1/\langle k \rangle = 1/[(N-1)f]$ (where f is the probability of existence of an edge), and thus the following relation should hold:

$$\frac{1}{(N-1)p_c} + \frac{1}{(N-1)\bar{p}_c} \simeq 1 \quad (4.2)$$

(an analogous complement relation of the two critical points also holds for regular graphs). The heuristics behind eq. (4.2) can indeed be extended also to the case of Erdős-Rényi multilayer networks. As a matter of fact if we consider two Erdős-Rényi layers of same size $N/2$ and densities p_1 and p_2 , connected by an Erdős-Rényi interaction matrix of density q ¹, we can use the first-order correction to the leading eigenvalue of the adjacency matrix of eq. (2.27) and write the relation:

$$\frac{\lambda_{max}^A + \bar{\lambda}_{max}^A}{N} = \frac{1}{2} \left(1 + \sqrt{\frac{\Delta^2}{4} + q^2} + \sqrt{\frac{\Delta^2}{4} + (1-q)^2} \right), \quad (4.3)$$

where $\Delta = |p_1 - p_2|$.

As we can see from eq. (4.3) if $\Delta = 0$ (hence when $p_1 = p_2$) we essentially end up with the same approximation given by eq. (4.2). On the other hand when Δ is large compared to q or $1 - q$ (due to the $q \leftrightarrow 1 - q$ symmetry) we have a non trivial correction to $(\lambda_{max}^A + \bar{\lambda}_{max}^A)/N$, up to a maximum value of $(3 + \sqrt{5})/4 \simeq 1.31$ which is realized in the extreme cases ($q = 0, \Delta = 1$) and ($q = 1, \Delta = 1$) (see figure 21).

As Figure 22 shows, eq. (4.2) slightly overestimates the relation between p_c and \bar{p}_c , as they do not add up to unity. In particular, the theoretical curve seems to constitute a boundary in the (p_c, \bar{p}_c) plane, and data are better fitted by a shifted linear relation

$$\frac{1}{(N-1)p_c} + \frac{1}{(N-1)\bar{p}_c} = \alpha < 1, \quad (4.4)$$

with $\alpha = 0.889 \pm 0.008$ and $\chi^2/\nu = 3.68$. The same behavior is observed in Figure 23 for theoretical values of the percolation threshold, obtained as the inverse of leading eigenvalue of the non-backtracking matrices (KNZ14a).

Building on the analysis of Figure 20, we then studied the relation

$$p_c + \bar{p}_c = \frac{1}{\beta'} \left(\frac{1}{\lambda_{max}} + \frac{1}{\bar{\lambda}_{max}} \right). \quad (4.5)$$

¹The complement graph is obtained by performing the substitutions $p_1 \rightarrow 1 - p_1, p_2 \rightarrow 1 - p_2, q \rightarrow 1 - q$.

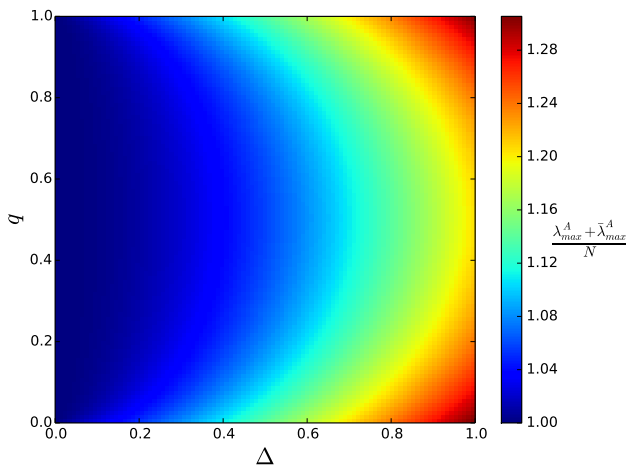


Figure 21: Heatmap representing eq. 4.3, with $0 \leq \Delta \leq 1$ and $0 \leq q \leq 1$.

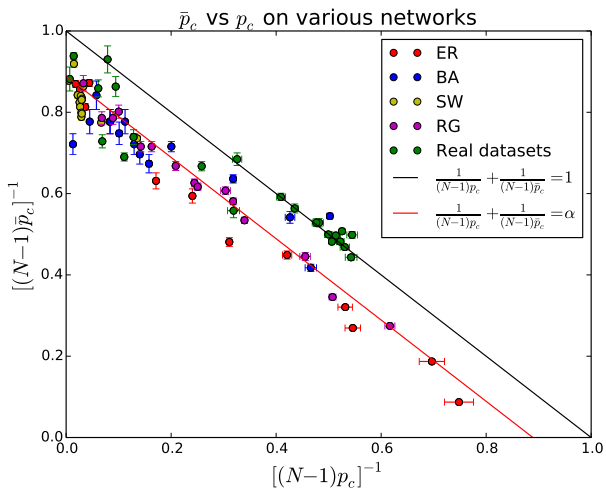


Figure 22: Plot of p_c^{-1} versus \bar{p}_c^{-1} for various networks of different sizes. The solid black line is eq. (4.2), while the solid red line is the linear fit of data.

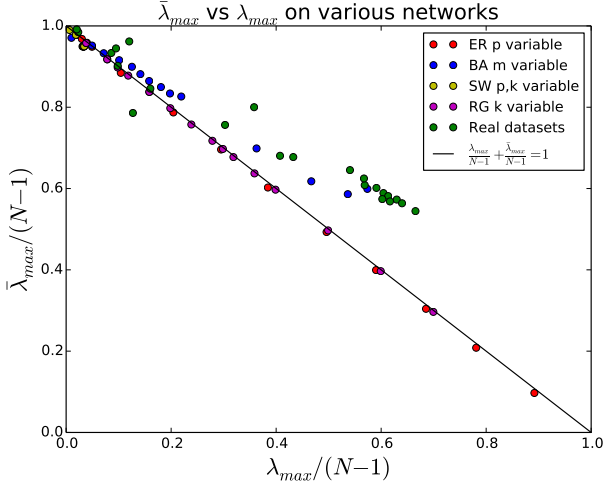


Figure 23: Plot of λ_{max} versus $\bar{\lambda}_{max}$ for various networks of different sizes.

As shown in Figure 24, eqn.(4.5) fits the data quite well, and much better than the fit of Figure 20. From the fit we obtained $\beta' = 0.856 \pm 0.010$ and $\chi^2/\nu = 1.16$. This factor can therefore be used to improve the estimate of the percolation threshold on finite, non treelike networks.

To show that this is the case, in Figure (25) we compare different estimates of the numerical percolation threshold, obtained as either the leading eigenvalues of the adjacency matrix λ_{max}^A or of the non-backtracking matrix λ_{max}^{NB} , eventually corrected by the β' factor. We indeed see that β' can be used to improve, on average, the approximation given by theoretical models.

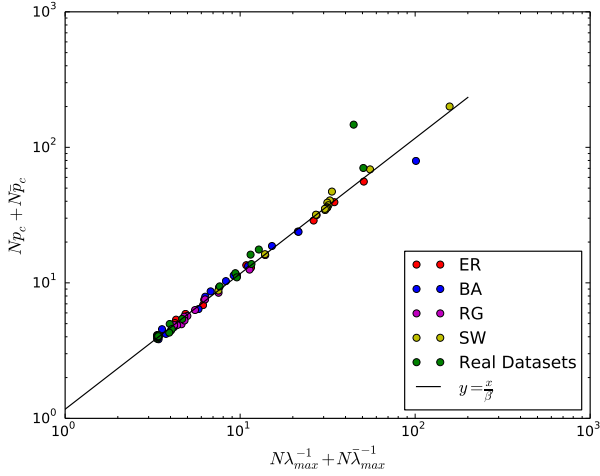


Figure 24: Plot of $Np_c + N\bar{p}_c$ vs $\left(\frac{N}{\lambda_{max}} + \frac{N}{\bar{\lambda}_{max}}\right)$, where λ_{max} is the leading eigenvalue of the non-backtracking matrix, for several model and empirical networks. The black solid line is the linear fit of eq. (4.5).

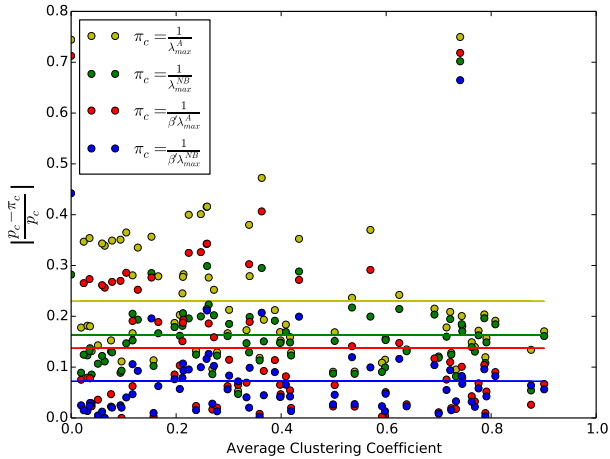


Figure 25: Relative error associated to different estimates for the percolation threshold. Solid lines indicates average values of dots of the same color.

Chapter 5

Conclusions

Here we summarize all the results presented in the previous chapters and discuss their practical relevance as well as possible future developments.

In Chapter 2 we employed a perturbative approach in order to study the connectivity properties for a general class of interacting multilayer networks. We generalized previous results (RA13; MHWMD14; DSSVM15) showing the presence of multiple structural transitions (*i.e.* multiple eigenvalue crossings in the algebraic connectivity) for interacting networks as interconnections are formed. This fact has a direct consequence on many physical dynamical systems which are governed by the laplacian spectrum, *e.g.*, diffusive processes. We have shown that beyond the first eigenvalue crossing, there might be as much as $Z - 1$ additional transitions, where Z is the number of network layers. In each of these regimes, the relaxation time of a diffusive processes on the entire system is set by a single layer. We further showed that, at first order in perturbation theory, the growth of the algebraic connectivity of each network layer depends only on the degree sequence of the interactions (projected on the respective Fiedler vector), and not on the actual interaction topology. We finally showed results of perturbation theory applied to the adjacency matrix of the interconnected network, which can be rather useful to identify percolation transitions on strongly interacting networks.

These findings have, therefore, important implications in the design of robust interconnected networked system, particularly when the functioning of the entire system crucially depends on one or a few network layers.

In Chapter 3 we dealt with bond percolation properties of interacting networks, with a particular attention to weakly interacting ones. This class of systems encompass the very important cases of multilayer/modular networks with very sparse connections within the layers/modules. We reported the existence of discontinuous jumps in the relative size of the giant component S , happening since the percolating cluster of the sparser layer can give either a full or zero contribution to the giant cluster of the whole system. Furthermore we observed that in this case the abrupt transition does not have a definite threshold, but can occur for a wide range of values of the bond occupation probability. This causes an anomalous behaviour of the susceptibility, which we captured using simple probabilistic arguments. We successfully tested our predictions in both synthetic and real systems. Finally, from finite-size scaling analysis we showed that the critical behaviour of both S and χ in the abrupt region exhibits the features of a genuine first-order phase transition. These results may change our understanding of the fragility of weakly interacting structures, since we are able to predict when abrupt first-order transitions (such as catastrophic failures) are more likely to occur. Concrete implications of our results apply to neural systems (with a major relevance to understand the resilience of neural processing), multiplex transportation networks, as well as networks with metapopulation structures (WX12b; SSC13; HSMS13; WTSA14; RTGX17).

Finally in Chapter 4 we presented an in-depth study conducted on both synthetic and real network datasets, which allows us to propose a method to correct the numerical estimate of the percolation threshold. We first showed the existence of an empirical linear relation between the observed threshold and its model predicted value across a large number of real and model networks and subsequently we explored the possibility

to improve such an empirical relation using the concept of complement graph. More precisely, we revealed the existence of an empirical linear relation between the inverse of the percolation threshold of a given graph and that of its complement. This relation applies to both single and multilayer structures and can eventually be used in order to build a more accurate estimate to the observed value of the percolation threshold. We believe that the corrective factor β' is related to finite size effects and non treelike structures, however this hypothesis needs further investigation. Overall, while our approach is just at infant stage and our findings are only preliminary, they may have important concrete applications.

To conclude, with this thesis we present new important results in the field of critical phenomena in multilayer network structures. Our findings provide both numerical and analytical tools which can be applied in the understanding of diffusion of epidemics, catastrophic failures, habits adoption, information, opinions in our multilayer-structured societies.

Appendix A

Perturbation Theory

A.1 Nondegenerate Case

Here we recall the basic notions of Perturbation Theory (PT) that we used in Chapter 2.

In PT we consider a given operator H to be represented as the sum of an unperturbed part H_0 and a perturbation V multiplied by a factor λ which indicates the strength of the perturbation, therefore

$$H = H_0 + \lambda V. \tag{A.1}$$

From here on we assume H to be symmetric, or self-adjoint in the case of complex entries. This is indeed the case of Laplacian and Adjacency matrices for undirected graphs, as well as the case of the eigenvalue problem for the time-independent Schrödinger equation in quantum mechanics (Sak94). In general, the same approach can be further extended to the case of non-symmetric matrices (Mar01).

Since H_0 is symmetric we assume to know the unperturbed *real* spectrum $E_n^{(0)}$ together with its corresponding set of orthogonal and normalized eigenvectors $|n^{(0)}\rangle$, which overall satisfies:

$$H_0 |n^{(0)}\rangle = E_n^{(0)} |n^{(0)}\rangle. \tag{A.2}$$

We then seek the solution of the perturbed system

$$H |n\rangle_\lambda = E_n^{(\lambda)} |n\rangle_\lambda \quad (\text{A.3})$$

in the form:

$$|n\rangle_\lambda = |n^{(0)}\rangle + \lambda |n^{(1)}\rangle + \lambda^2 |n^{(2)}\rangle + \dots, \quad (\text{A.4})$$

$$E_n^{(\lambda)} = E_n^{(0)} + \lambda \epsilon_n^{(1)} + \lambda^2 \epsilon_n^{(2)} + \dots \quad (\text{A.5})$$

Let's now assume $E_n^{(0)}$ to be non-degenerate: by substituting eqs. (A.5) (A.4) (A.1) into eq. (A.3) and keeping only the terms at most proportional to λ , we easily get the first-order correction:

$$\epsilon_n^{(1)} = \langle n^{(0)} | V | n^{(0)} \rangle \quad (\text{A.6})$$

together with the new set of normalized eigenstates:

$$|n^{(1)}\rangle = \sum_{k \neq n} |k\rangle \frac{1}{E_n^{(0)} - E_k^{(0)}} \langle k | V | n^{(0)} \rangle, \quad (\text{A.7})$$

where $|k\rangle$ here indicates are the normalized eigenstates of H_0 . As we can see from eq. (A.7), the assumption of having a non-degenerate unperturbed spectrum is fundamental otherwise at least one of the vectors belonging to the first-order set $|n^{(1)}\rangle$ would present a divergent term.

In order to compute the second-order solution we need both the first-order and the unperturbed solution. In general the system can be solved recursively, and the solution to the L -th order is given by:

$$\epsilon_n^{(L)} = \langle n^{(0)} | V | n^{(L-1)} \rangle. \quad (\text{A.8})$$

For instance the second-order correction reads:

$$\epsilon_n^{(2)} = \langle n^{(0)} | V | n^{(1)} \rangle = \sum_{k \neq n} \frac{|\langle k | V | n^{(0)} \rangle|^2}{E_n^{(0)} - E_k^{(0)}}. \quad (\text{A.9})$$

Note that at every order in perturbation theory there is no explicit dependency on λ . As a matter of fact λ is only needed in order to identify each approximation regime, but it doesn't affect the final results concretely. In most applications λ is in fact usually replaced by unity (Mar01).

A.2 Degenerate Case

As we said here above, if the unperturbed spectrum $E_n^{(0)}$ is degenerate, then equation (A.7) and higher order corrections might diverge, therefore we need to take a different approach. In fact we are going to assume that in this case the perturbation only mixes the degenerate states, therefore we are going to solve the problem exactly for that subset of states. Let's assume that H_0 posses $g_0 \in \mathbb{N}$ degenerate eigenstates $|m\rangle$, with respect to the degenerate eigenvalue $E_D^{(0)}$. We now assume that a generic perturbed eigenstate $|\psi_j\rangle$ belongs to the degenerate eigenspace spanned by $|m\rangle$, hence:

$$|\psi_j\rangle = \sum_i |m_i\rangle \langle m_i | \psi_j \rangle = \sum_i c_{ij} |m_i\rangle, \quad (\text{A.10})$$

where we used the identity $\sum_i |m_i\rangle \langle m_i| = \mathbb{1}$.

Having set $\lambda = 1$, eq. (A.1) applied to ψ_j then reads:

$$(H_0 + V) |\psi_j\rangle = (H_0 + V) \sum_i c_{ij} |m_i\rangle = E_j \sum_i c_{ij} |m_i\rangle.$$

Since by assumption $H_0 |m_i\rangle = E_D^{(0)} |m_i\rangle$, we easily obtain:

$$\sum_i c_{ij} \left[\langle m_k | V | m_i \rangle - \delta_{ik} (E_j - E_D^{(0)}) \right] = 0, \quad (\text{A.11})$$

where we used $\langle m_k | m_i \rangle = \delta_{ik}$.

If we now define the projection of the perturbation onto the degenerate subspace $\tilde{V}_{ij} \equiv \langle m_k | V | m_i \rangle$ and the corrections $\epsilon_j^{(1)} \equiv E_j - E_D^{(0)}$, eq. (A.11) is then satisfied if and only if:

$$\det(\tilde{V} - \epsilon^{(1)} \mathbb{1}) = 0. \quad (\text{A.12})$$

Note that eq. (A.12) correctly reduces to eq. (A.6) in the case of \tilde{V} being one-dimensional, *i.e.* in the non-degenerate case. In general the secular equation (A.12) admits g_0 roots: in case they are all distinct the degeneracy is then *completely* lifted, otherwise is only *partially* lifted.

To conclude, if the unperturbed spectrum presents several degenerate eigenvalues we first project the perturbation onto each degenerate subspace and solve eq. (A.12) until each degeneracy is completely lifted,

or equivalently for each degenerate subspace we find a new basis which diagonalizes \tilde{V} . At the same time we apply standard non-degenerate perturbation theory to the rest of the spectrum.

Appendix B

Definition and main properties of the complement network

Formally, let A_{ij} be the generic element of the adjacency matrix A associated with a given binary undirected graph G of N vertices, such that $A_{ij} = 1$ if an edge between vertices i and j exists, and $A_{ij} = 0$ otherwise. The adjacency matrix of the complement graph \bar{G} is defined through

$$\bar{A}_{ij} = 1 - \delta_{ij} - A_{ij}, \quad (\text{B.1})$$

where δ_{ij} is the Kronecker delta which excludes self loops from \bar{G} , and $1 - \delta_{ij} \equiv K_{ij}$ defines the adjacency matrix of the complete graph.

From definition (B.1) it follows trivially that

$$k_i + \bar{k}_i = N - 1 \quad \forall i \quad (\text{B.2})$$

$$E + \bar{E} = \binom{N}{2} \quad (\text{B.3})$$

$$\rho + \bar{\rho} = 1, \quad (\text{B.4})$$

where k_i , E and ρ denote the degree of (number of edges incident with) generic vertex i , the number of edges and the edge density respectively.

Thus, given the degree distribution $P(k)$, the distribution of the complement degree is obtained as

$$\bar{P}(\bar{k}) = P(N - 1 - \bar{k}), \quad (\text{B.5})$$

i.e., as the reflection of $P(k)$ on the $\frac{N-1}{2}$ vertical axis. Notably, the degree distribution of both a regular graph and an Erdős-Rényi graph (ER) are invariant under this transformation: the complement of a regular graph is a regular graph, as the complement of an ER is an ER. In particular, the complement of an ER with connection probability f is an ER with connection probability $1 - f$.

Moving to higher-order properties, we consider the relation between the number of triangles (closed loop of length 3) of a graph, which is given by $\frac{\text{Tr}A^3}{6}$, and that of its complement. We then define the quantity:

$$\Sigma_{\Delta} \equiv \frac{\text{Tr}A^3 + \text{Tr}\bar{A}^3}{6}.$$

By direct substitution of eq. B.1 we obtain:

$$\Sigma_{\Delta} = \binom{N}{3} - \frac{1}{2} \sum_i k_i \bar{k}_i. \quad (\text{B.6})$$

As such, both cases $k_i = 0$ and $\bar{k}_i = 0 \forall i$ (empty and complete graph) lead to $\Sigma_{\Delta} = \binom{N}{3}$ as expected. Furthermore note that the degree configuration that minimizes Σ_{Δ} is the one a regular graph with $k_i = \frac{N-1}{2}$. As a matter of fact:

$$\frac{\partial \Sigma_{\Delta}}{\partial k_j} = -\frac{1}{2} \sum_i [\delta_{ij}(N - 1 - 2k_i)] \stackrel{!}{=} 0 \Leftrightarrow k_j = \frac{N - 1}{2}.$$

This configuration is indeed a local minimum since $\frac{\partial \Sigma_{\Delta}}{\partial k_i \partial k_j} = 1$.

As for transitivity, a complementarity relation can be written also for the local clustering coefficient $c_i = \frac{\sum_{j \neq i} \sum_{k \neq i, j} A_{ij} A_{jk} A_{ik}}{k_i(k_i - 1)}$:

$$c_i k_i (k_i - 1) + \bar{c}_i \bar{k}_i (\bar{k}_i - 1) = k_i^{nn} k_i + \bar{k}_i^{nn} \bar{k}_i - k_i - \bar{k}_i - k_i \bar{k}_i, \quad (\text{B.7})$$

where $k_i^{nn} = \frac{\sum_{j \neq i} A_{ij} k_j}{k_i}$ is the average nearest-neighbors degree.

References

- [ADG07] Juan A Almendral and Albert Díaz-Guilera. Dynamical and spectral properties of complex networks. *New Journal of Physics*, 9(6):187, 2007. 21
- [ADGK⁺08] Alex Arenas, Albert Díaz-Guilera, Jurgen Kurths, Yamir Moreno, and Changsong Zhou. Synchronization in complex networks. *Physics Reports*, 469(3):93–153, 2008. 7, 21
- [ADS09] Dimitris Achlioptas, Raissa M. D’Souza, and Joel Spencer. Explosive percolation in random networks. *Science*, 323(5920):1453–1455, 2009. 42
- [AH79] Jin Akiyama and Frank Harary. A graph and its complement with specified properties i: connectivity. *International Journal of Mathematics and Mathematical Sciences*, 2(2):223–228, 1979. 57
- [ASEG⁺14] J. Aguirre, R. Sevilla-Escoboza, R. Gutiérrez, D. Papo, and J. M. Buldú. Synchronization of interconnected networks: The role of connector nodes. *Physical Review Letters*, 112:248701, 2014. 20
- [BBC⁺14] S. Boccaletti, G. Bianconi, R. Criado, C.I. del Genio, J. Gómez-Gardeñes, M. Romance, I. Sendi na Nadal, Z. Wang, and M. Zanin. The structure and dynamics of multilayer networks. *Physics Reports*, 544(1):1–122, 2014. 20
- [BBCR10a] B. Bollobás, C. Borgs, J. Chayes, and O. Riordan. Percolation on dense graph sequences. *The Annals of Probability*, 38(1):150–183, 2010. 36
- [BBCR10b] Béla Bollobás, Christian Borgs, Jennifer Chayes, and Oliver Riordan. Percolation on dense graph sequences. *The Annals of Probability*, 38(1):150–183, 2010. 57

- [BBdC⁺16] Gareth J. Baxter, Ginestra Bianconi, Rui A. da Costa, Sergey N. Dorogovtsev, and José F. F. Mendes. Correlated edge overlaps in multiplex networks. *Physical Review E*, 94:012303, 2016. 39
- [BD14] Ginestra Bianconi and Sergey N. Dorogovtsev. Multiple percolation transitions in a configuration model of a network of networks. *Physical Review E*, 89:062814, 2014. 20, 38
- [BDGM12] G. J. Baxter, S. N. Dorogovtsev, A. V. Goltsev, and J. F. F. Mendes. Avalanche collapse of interdependent networks. *Physical Review Letters*, 109:248701, 2012. 38
- [Bol81] Béla Bollobás. Degree sequences of random graphs. *Discrete Mathematics*, 33(1):1–19, 1981. 30
- [BPP⁺10] Sergey V Buldyrev, Roni Parshani, Gerald Paul, H. Eugene Stanley, and Shlomo Havlin. Catastrophic cascade of failures in interdependent networks. *Nature*, 464:1025, 2010. 20, 38
- [BRST11] Sergio Bermudo, José M. Rodríguez, José M. Sigarreta, and Eva Tours. Hyperbolicity and complement of graphs. *Applied Mathematics Letters*, 24(11):1882–1887, 2011. 57
- [CbAH02a] Reuven Cohen, Daniel ben Avraham, and Shlomo Havlin. Percolation critical exponents in scale-free networks. *Physical Review E*, 66:036113, 2002. 38
- [CbAH02b] Reuven Cohen, Daniel ben Avraham, and Shlomo Havlin. Percolation critical exponents in scale-free networks. *Physical Review E*, 66:036113, 2002. 54
- [CdSBn14] Pol Colomer-de Simón and Marián Boguñá. Double percolation phase transition in clustered complex networks. *Physical Review X*, 4:041020, 2014. 36, 39, 44, 48, 53
- [CE83] L. Clark and R. Entringer. Smallest maximally nonhamiltonian graphs. *Periodica Mathematica Hungarica*, 14(1):57–68, 1983. 57
- [CGGZ⁺13] Alessio Cardillo, Jess Gómez-Gardees, Massimiliano Zanin, Miguel Romance, David Papo, Francisco del Pozo, and Stefano Boccaletti. Emergence of network features from multiplexity. *Scientific Reports*, 3(1344), 2013. 46
- [CGO09] Sanjeev Chauhan, Michelle Girvan, and Edward Ott. Spectral properties of networks with community structure. *Physical Review E*, 80:056114, 2009. 22, 27

- [CLZ⁺13] Davide Cellai, Eduardo López, Jie Zhou, James P. Gleeson, and Ginestra Bianconi. Percolation in multiplex networks with overlap. *Physical Review E*, 88:052811, 2013. 39
- [CNSW00] Duncan S. Callaway, M. E. J. Newman, Steven H. Strogatz, and Duncan J. Watts. Network robustness and fragility: Percolation on random graphs. *Physical Review Letters*, 85:5468–5471, 2000. 38
- [CPS10] Claudio Castellano and Romualdo Pastor-Satorras. Thresholds for epidemic spreading in networks. *Physical Review Letters*, 105:218701, 2010. 38
- [CSN09] Aaron Clauset, Cosma Rohilla Shalizi, and Mark E. J. Newman. Power-law distributions in empirical data. *SIAM Review*, 51:661–703, 2009. 13
- [DDGPA16] Manlio De Domenico, Clara Granell, Mason A Porter, and Alex Arenas. The physics of spreading processes in multilayer networks. *Nature Physics*, 12:901, 2016. 18, 20
- [DDSRC⁺13] Manlio De Domenico, Albert Solé-Ribalta, Emanuele Cozzo, Mikko Kivelä, Yamir Moreno, Mason A. Porter, Sergio Gómez, and Alex Arenas. Mathematical formulation of multilayer networks. *Physical Review X*, 3:041022, 2013. 18, 20
- [DDSRGA14] Manlio De Domenico, Albert Solé-Ribalta, Sergio Gómez, and Alex Arenas. Navigability of interconnected networks under random failures. *Proceedings of the National Academy of Sciences*, 111(23):8351–8356, 2014. 20
- [DGM08] S. N. Dorogovtsev, A. V. Goltsev, and J. F. F. Mendes. Critical phenomena in complex networks. *Review of Modern Physics*, 80:1275–1335, 2008. 17
- [DHS12] Mark Dickison, S. Havlin, and H. E. Stanley. Epidemics on interconnected networks. *Physical Review E*, 85:066109, 2012. 20, 39
- [DLC08] Zhisheng Duan, Chao Liu, and Guanrong Chen. Network synchronizability analysis: The theory of subgraphs and complementary graphs. *Physica D: Nonlinear Phenomena*, 237(7):1006–1012, 2008. 57
- [DLR15] Jean-Charles Delvenne, Renaud Lambiotte, and Luis E. C. Rocha. Diffusion on networked systems is a question of time or structure. *Nature Communications*, 6:7366, 2015. 31

- [DN15] Raissa M. DSouza and Jan Nagler. Anomalous critical and supercritical phenomena in explosive percolation. *Nature Physics*, 11:531, 2015. 42
- [DSSVM15] Faryad Darabi Sahneh, Caterina Scoglio, and Piet Van Mieghem. Exact coupling threshold for structural transition reveals diversified behaviors in interconnected networks. *Physical Review E*, 92:040801, 2015. 20, 22, 27, 62
- [EGGn14] Ernesto Estrada and Jesús Gómez-Gardeñes. Communicability reveals a transition to coordinated behavior in multiplex networks. *Physical Review E*, 89:042819, 2014. 20
- [Fie75] M. Fielder. A property of eigenvectors of nonnegative symmetric matrices and its application to graph theory. *Linear Algebra and its Applications*, 25(619), 1975. 21
- [FL09] Eric J. Friedman and Adam S. Landsberg. Construction and analysis of random networks with explosive percolation. *Physical Review Letters*, 103:255701, 2009. 42
- [FMCdSG16] Ali Faqeeh, Sergey Melnik, Pol Colomer-de Simón, and James P. Gleeson. Emergence of coexisting percolating clusters in networks. *Physical Review E*, 93:062308, 2016. 40, 43
- [Fri03] Joel Friedman. A proof of alon’s second eigenvalue conjecture. In *Proceedings of the Thirty-fifth Annual ACM Symposium on Theory of Computing, STOC ’03*, pages 720–724, New York, NY, USA, 2003. ACM. 35
- [Gar16] Antonios Garas, editor. *Interconnected Networks. Understanding Complex Systems*. Springer International Publishing, 2016. 20
- [GBHS11] Jianxi Gao, Sergey V. Buldyrev, Shlomo Havlin, and H. Eugene Stanley. Robustness of a network of networks. *Physical Review Letters*, 107:195701, 2011. 20, 38
- [GCB⁺11] Peter Grassberger, Claire Christensen, Golnoosh Bizhani, Seung-Woo Son, and Maya Paczuski. Explosive percolation is continuous, but with unusual finite size behavior. *Physical Review Letters*, 106:225701, 2011. 42
- [GDGGGn⁺13] S. Gómez, A. Díaz-Guilera, J. Gómez-Gardeñes, C. J. Pérez-Vicente, Y. Moreno, and A. Arenas. Diffusion dynamics on multiplex networks. *Physical Review Letters*, 110:028701, 2013. 20, 22

- [GDM03] A. V. Goltsev, S. N. Dorogovtsev, and J. F. F. Mendes. Critical phenomena in networks. *Physical Review E*, 67:026123, 2003. 12, 13, 15
- [GGA13] Clara Granell, Sergio Gómez, and Alex Arenas. Dynamical interplay between awareness and epidemic spreading in multiplex networks. *Physical Review Letters*, 111:128701, 2013. 20
- [GGDDG⁺15] J. Gómez-Gardeñes, M. De Domenico, G. Gutiérrez, A. Arenas, and S. Gómez. Layer-layer competition in multiplex complex networks. *Philosophical Transactions of the Royal Society of London A*, 373(2056), 2015. 20
- [Gra83] P. Grassberger. On the critical behavior of the general epidemic process and dynamical percolation. *Mathematical Biosciences*, 63, 1983. 13
- [GY98] J.L. Gross and J. Yellen. *Graph Theory and Its Applications*. Discrete Mathematics and Its Applications. Taylor & Francis, 1998. 57
- [HCG⁺16] A. Hackett, D. Cellai, S. Gómez, A. Arenas, and J. P. Gleeson. Bond percolation on multiplex networks. *Phys. Rev. X*, 6:021002, 2016. 20, 36, 39
- [HI97] Frank C. Hoppensteadt and Eugene M. Izhikevich. *Weakly Connected Neural Networks*. Springer-Verlag, 1997. 39
- [HKCH11] Yanqing Hu, Baruch Ksherim, Reuven Cohen, and Shlomo Havlin. Percolation in interdependent and interconnected networks: Abrupt change from second- to first-order transitions. *Physical Review E*, 84:066116, 2011. 20
- [HN14] K. Hashimoto and Y. Namikawa. *Automorphic Forms and Geometry of Arithmetic Varieties*. Advanced Studies in Pure Mathematics. Elsevier Science, 2014. 54
- [HN17] Shigefumi Hata and Hiroya Nakao. *Scientific Reports*, 7:1121, 2017. 22
- [HP14] Kathleen E. Hamilton and Leonid P. Pryadko. Tight lower bound for percolation threshold on an infinite graph. *Physical Review Letters*, 113:208701, 2014. 54
- [HPL⁺06] Liang Huang, Kwangho Park, Ying-Cheng Lai, Lei Yang, and Kongqing Yang. Abnormal synchronization in complex clustered networks. *Physical Review Letters*, 97:164101, 2006. 20

- [HSMS13] Jason Hindes, Sarabjeet Singh, Christopher R. Myers, and David J. Schneider. Epidemic fronts in complex networks with metapopulation structure. *Physical Review E*, 88:012809, 2013. 63
- [Hua87] Kerson Huang. *Statistical mechanics / Kerson Huang*. Wiley New York, 2nd ed. edition, 1987. 9
- [HW04] Ruth Haas and Thomas B. Wexler. Signed domination numbers of a graph and its complement. *Discrete Mathematics*, 283(1):87–92, 2004. 57
- [HZZ⁺13] Yanqing Hu, Dong Zhou, Rui Zhang, Zhangang Han, Céline Rozenblat, and Shlomo Havlin. Percolation of interdependent networks with intersimilarity. *Physical Review E*, 88:052805, 2013. 39
- [IY98] Hiro Ito and Mitsuo Yokoyama. Linear time algorithms for graph search and connectivity determination on complement graphs. *Information Processing Letters*, 66(4):209–213, 1998. 57
- [JVM08] A. Jamakovic and Piet Van Mieghem. *On the Robustness of Complex Networks by Using the Algebraic Connectivity*, pages 183–194. Springer, Berlin Heidelberg, 2008. 7, 21, 26, 30
- [KAB⁺14] Mikko Kivelä, Alex Arenas, Marc Barthélemy, James P. Gleeson, Yamir Moreno, and Mason A. Porter. Multilayer networks. *Journal of Complex Networks*, 2(3):203–271, 2014. 20
- [KM07] Dong-Hee Kim and Adilson E. Motter. Ensemble averageability in network spectra. *Physical Review Letters*, 98:248701, 2007. 22
- [KNZ14a] Brian Karrer, M. E. J. Newman, and Lenka Zdeborová. Percolation on sparse networks. *Physical Review Letters*, 113:208702, Nov 2014. 45, 46, 58
- [KNZ14b] Brian Karrer, M. E. J. Newman, and Lenka Zdeborová. Percolation on sparse networks. *Physical Review Letters*, 113:208702, 2014. 54
- [KOT98] Ming-Yang Kao, Neill Occhiogrosso, and Shang-Hua Teng. Simple and efficient graph compression schemes for dense and complement graphs. *Journal of Combinatorial Optimization*, 2(4):351–359, 1998. 57
- [LCS⁺16] Deokjae Lee, S. Choi, M. Stippinger, J. Kertész, and B. Kahng. Hybrid phase transition into an absorbing state: Percolation and avalanches. *Physical Review E*, 93:042109, Apr 2016. 39

- [LD09] E. A. Leicht and Raissa M. D’Souza. Percolation on interacting networks. <https://arxiv.org/abs/0907.0894>, 2009. 39
- [LESL18] Run-Ran Liu, Daniel A Eisenberg, Thomas P Seager, and Ying-Cheng Lai. The “weak” interdependence of infrastructure systems produces mixed percolation transitions in multilayer networks. *Scientific Reports*, 8(1):2111, 2018. 39
- [LLJW13] Ming Li, Run-Ran Liu, Chun-Xiao Jia, and Bing-Hong Wang. Critical effects of overlapping of connectivity and dependence links on percolation of networks. *New Journal of Physics*, 15(9):093013, 2013. 39
- [Mar01] R. A. Marcus. Brief comments on perturbation theory of a non-symmetric matrix:the gf matrix. *The Journal of Physical Chemistry A*, 105(12):2612–2616, 2001. 65, 66
- [MHWMD14] J. Martín-Hernández, H. Wang, P. Van Mieghem, and G. D’Agostino. Algebraic connectivity of interdependent networks. *Physica A: Statistical Mechanics and its Applications*, 404(Supplement C):92–105, 2014. 20, 22, 26, 27, 29, 62
- [Moh91] B Mohar. The laplacian spectrum of graphs. In Y Alavi, G Chartrand, O R Oellermann, and A J Schwenk, editors, *Graph Theory, Combinatorics, and Applications*, Proceedings of the Sixth Quadrennial International Conference on the Theory and Applications of Graphs, pages 871–898. Wiley, New York, 1991. 21
- [MPL17] Naoki Masuda, Mason A. Porter, and Renaud Lambiotte. Random walks and diffusion on networks. *Physics Reports*, 716-717:1–58, 2017. 31
- [MPMG14] Sergey Melnik, Mason A. Porter, Peter J. Mucha, and James P. Gleeson. Dynamics on modular networks with heterogeneous correlations. *Chaos: An Interdisciplinary Journal of Nonlinear Science*, 24(2):023106, 2014. 39
- [NAC14] M. Nitti, L. Atzori, and I. P. Cvijikj. Network navigability in the social internet of things. In *2014 IEEE World Forum on Internet of Things (WF-IoT)*, pages 405–410, March 2014. 7
- [NdA07] Maria Nair and Maia de Abreu. Old and new results on algebraic connectivity of graphs. *Czech. Math. J.*, 423:53–73, 2007. 7
- [New02] M. E. J. Newman. Spread of epidemic disease on networks. *Phys. Rev. E*, 66:016128, Jul 2002. 13

- [New03] M. E. J. Newman. The structure and function of complex networks. *SIAM Review*, 45(2):167–256, 2003. 55
- [New09] M. E. J. Newman. Random graphs with clustering. *Physical Review Letters*, 103:058701, 2009. 54
- [NG56] E. A. Nordhaus and J. W. Gaddum. On complementary graphs. *The American Mathematical Monthly*, 63(3):175–177, 1956. 57
- [NLT11] Jan Nagler, Anna Levina, and Marc Timme. Impact of single links in competitive percolation. *Nature Physics*, 7:265, 2011. 42
- [NSW01] M. E. J. Newman, S. H. Strogatz, and D. J. Watts. Random graphs with arbitrary degree distributions and their applications. *Physical Review E*, 64:026118, 2001. 38
- [NTG12] Jan Nagler, Tyge Tjessen, and Harold W. Gutch. Continuous percolation with discontinuities. *Physical Review X*, 2:031009, 2012. 42
- [NZ00a] M. E. J. Newman and R. M. Ziff. Efficient monte carlo algorithm and high-precision results for percolation. *Physical Review Letters*, 85:4104–4107, 2000. 40
- [NZ00b] M. E. J. Newman and R. M. Ziff. Efficient monte carlo algorithm and high-precision results for percolation. *Physical Review Letters*, 85:4104–4107, 2000. 55
- [PBH11] Roni Parshani, Sergey V. Buldyrev, and Shlomo Havlin. Critical effect of dependency groups on the function of networks. *Proceedings of the National Academy of Sciences*, 108(3):1007–1010, 2011. 38
- [PRS03] M. Petrović, Z. Radosavljević, and S. Simić. A graph and its complement with specified spectral properties. *Linear and Multilinear Algebra*, 51(4):405–419, 2003. 57
- [PSCMV14] Romualdo Pastor-Satorras, Claudio Castellano, Piet Van Mieghem, and Alessandro Vespignani. Epidemic processes in complex networks. *CoRR*, abs/1408.2701, 2014. 12, 13
- [RA13] Filippo Radicchi and Alex Arenas. Abrupt transition in the structural formation of interconnected networks. *Nature Physics*, 9:717, 2013. 20, 21, 23, 27, 62

- [RACC18a] Giacomo Rapisardi, Alex Arenas, Guido Caldarelli, and Giulio Cimini. Fragility and anomalous susceptibility of weakly interacting networks. <https://arxiv.org/abs/1810.01250>, 2018. 18
- [RACC18b] Giacomo Rapisardi, Alex Arenas, Guido Caldarelli, and Giulio Cimini. Multiple structural transitions in interacting networks. *Phys. Rev. E*, 98:012302, Jul 2018. 18
- [Rad14] Filippo Radicchi. Driving interconnected networks to supercriticality. *Physical Review X*, 4:021014, 2014. 20
- [Rad15] Filippo Radicchi. Predicting percolation thresholds in networks. *Physical Review E*, 91:010801, 2015. 54
- [RB17] Filippo Radicchi and Ginestra Bianconi. Redundant interdependencies boost the robustness of multiplex networks. *Phys. Rev. X*, 7:011013, 2017. 39
- [RC15a] Filippo Radicchi and Claudio Castellano. Breaking of the site-bond percolation universality in networks. *Nature Communications*, 6:10196, 2015. 17, 38, 48
- [RC15b] Filippo Radicchi and Claudio Castellano. Breaking of the site-bond percolation universality in networks. *Nature Communications*, 6:10196, 2015. 55
- [RC16a] Filippo Radicchi and Claudio Castellano. Beyond the locally treelike approximation for percolation on real networks. *Physical Review E*, 93:030302, 2016. 18, 36
- [RC16b] Filippo Radicchi and Claudio Castellano. Beyond the locally treelike approximation for percolation on real networks. *Physical Review E*, 93:030302, 2016. 54
- [RF09] Filippo Radicchi and Santo Fortunato. Explosive percolation in scale-free networks. *Physical Review Letters*, 103:168701, Oct 2009. 50
- [RGG19] G. Rapisardi, Caldarelli G., and Cimini G. *Numerical Assessment of the Percolation Threshold Using Complementary Networks*, volume 812, pages 820–827. Springer, 2019. 19
- [RTGX17] Zhongyuan Ruan, Ming Tang, Changgui Gu, and Jinshan Xu. Epidemic spreading between two coupled subpopulations with inner structures. *Chaos: An Interdisciplinary Journal of Nonlinear Science*, 27(10):103104, 2017. 63

- [SADS⁺16] Heman Shakeri, Nathan Albin, Faryad Darabi Sahneh, Pietro Poggi-Corradini, and Caterina Scoglio. Maximizing algebraic connectivity in interconnected networks. *Physical Review E*, 93:030301, 2016. 20
- [Sak94] Jun John Sakurai. *Modern quantum mechanics; rev. ed.* Addison-Wesley, Reading, MA, 1994. 65
- [SBC⁺12] Seung-Woo Son, Golnoosh Bizhani, Claire Christensen, Peter Grassberger, and Maya Paczuski. Percolation theory on interdependent networks based on epidemic spreading. *EPL (Europhysics Letters)*, 97(1):16006, 2012. 38
- [SBn06] M. Ángeles Serrano and Marián Boguñá. Percolation and epidemic thresholds in clustered networks. *Physical Review Letters*, 97:088701, 2006. 18, 54
- [SDM08] A. N. Samukhin, S. N. Dorogovtsev, and J. F. F. Mendes. Laplacian spectra of, and random walks on, complex networks: Are scale-free architectures really important? *Physical Review E*, 77:036115, 2008. 21, 26
- [SGCM14] Rubén J. Sánchez-García, Emanuele Cozzo, and Yamir Moreno. Dimensionality reduction and spectral properties of multilayer networks. *Physical Review E*, 89:052815, 2014. 20
- [SKK⁺15] Saray Shai, Dror Y. Kenett, Yoed N. Kenett, Miriam Faust, Simon Dobson, and Shlomo Havlin. Critical tipping point distinguishing two types of transitions in modular network structures. *Physical Review E*, 92:062805, 2015. 39
- [SMSBn12] Anna Saumell-Mendiola, M. Ángeles Serrano, and Marián Boguñá. Epidemic spreading on interconnected networks. *Physical Review E*, 86:026106, 2012. 20
- [SRDDK⁺13] A. Solé-Ribalta, M. De Domenico, N. E. Kouvaris, A. Díaz-Guilera, S. Gómez, and A. Arenas. Spectral properties of the laplacian of multiplex networks. *Physical Review E*, 88:032807, 2013. 20, 22
- [SSC13] F. D. Sahneh, C. Scoglio, and F. N. Chowdhury. Effect of coupling on the epidemic threshold in interconnected complex networks: A spectral analysis. In *2013 American Control Conference*, pages 2307–2312, 2013. 63

- [TdCDM17] G. Timár, R. A. da Costa, S. N. Dorogovtsev, and J. F. F. Mendes. Nonbacktracking expansion of finite graphs. *Physical Review E*, 95:042322, 2017. 55
- [VM16] P. Van Mieghem. Interconnectivity structure of a general interdependent network. *Physical Review E*, 93:042305, 2016. 20, 22, 25, 26
- [WDF11] Yang Wang, Zengru Di, and Ying Fan. Identifying and characterizing nodes important to community structure using the spectrum of the graph. *PLoS ONE*, 6(11):1–10, 2011. 22
- [Wil06] Herbert S. Wilf. *Generatingfunctionology*. A. K. Peters, Ltd., Natick, MA, USA, 2006. 14, 15
- [WTSa14] Bing Wang, Gouhei Tanaka, Hideyuki Suzuki, and Kazuyuki Aihara. Epidemic spread on interconnected metapopulation networks. *Physical Review E*, 90:032806, 2014. 63
- [WX12a] Y. Wang and G. Xiao. Epidemics spreading in interconnected complex networks. *Physics Letters A*, 376(42):2689–2696, 2012. 20
- [WX12b] Y. Wang and G. Xiao. Epidemics spreading in interconnected complex networks. *Physics Letters A*, 376(42):2689 – 2696, 2012. 63
- [Xu87] Shao-ji Xu. Some parameters of graph and its complement. *Discrete Mathematics*, 65(2):197–207, 1987. 57
- [YWL⁺14] Xin Yan, Yang Wu, Xiaohui Li, Chunlin Li, and Yaogai Hu. Eigenvector perturbations of complex networks. *Physica A: Statistical Mechanics and its Applications*, 408(Supplement C):106–118, 2014. 22
- [ZB13a] Kun Zhao and Ginestra Bianconi. Percolation on interacting, antagonistic networks. *Journal of Statistical Mechanics: Theory and Experiment*, 2013(05):P05005, 2013. 39
- [ZB13b] Kun Zhao and Ginestra Bianconi. Percolation on interdependent networks with a fraction of antagonistic interactions. *Journal of Statistical Physics*, 152(6):1069–1083, 2013. 39



SOME RIGHTS RESERVED



Unless otherwise expressly stated, all original material of whatever nature created by Giacomo Rapisardi and included in this thesis, is licensed under a Creative Commons Attribution Noncommercial Share Alike 2.5 Italy License.

Check creativecommons.org/licenses/by-nc-sa/2.5/it/ for the legal code of the full license.

Ask the author about other uses.